

Opportunities, Challenges, and Strategies for Scalable Deposition of Metal Halide Perovskite Solar Cells and Modules

Azam Khorasani,* Faterme Mohamadkhani, Maziar Marandi, Huiming Luo, and Mojtaba Abdi-Jalebi*

Hybrid organic-inorganic perovskite solar cells (PSCs) have rapidly advanced in the new generation of photovoltaic devices. As the demand for energy continues to grow, the pursuit of more stable, highly efficient, and cost-effective solar cells has intensified in both academic research and the industry. Consequently, the development of scalable fabrication techniques that yield a uniform and dense perovskite absorber layer with optimal crystallization plays a crucial role to enhance stability and higher efficiency of perovskite solar modules. This review provides a comprehensive summary of recent advancements, comparison, and future prospects of scalable deposition techniques for perovskite photovoltaics. We discuss various techniques, including solution-based and physical methods such as blade coating, inkjet printing (IJP), screen printing, slot-die coating, physical vapor deposition, and spray coating that have been employed for fabrication of perovskite modules. The advantages and challenges associated with these techniques, such as contactless and maskless deposition, scalability, and compatibility with roll-to-roll processes, have been thoroughly examined. Finally, the integration of multiple subcells in perovskite solar modules is explored using different scalable deposition techniques.

1. Introduction

High efficiency and superb performance of hybrid organic-inorganic perovskite solar cells (PSCs) have attracted considerable research attention in recent years. Hybrid organic-inorganic perovskites with ABX_3 structure possess distinctive optoelectronic properties, including a direct and adjustable bandgap energy, low exciton binding energy, and a high absorption coefficient. Moreover, they demonstrate broadband light absorption,

ambipolar behavior, and long charge carrier diffusion length.^[1–4] These various optoelectronic properties can be modified by changing the composition of A, B, and X ions in perovskite structure.^[5–7] Application of perovskite materials as the light harvesting films has significantly increased the power conversion efficiency (PCE) of corresponding cells from 3.8% in 2009 to 26.08%.^[8–12]

The rapid progress in efficiency of PSCs has indicated that deposition techniques for the light-absorbing film, the electron transporting layers (ETLs) and hole transporting layers (HTLs), have extreme effects on related uniformity and surface quality, resulting in high efficiency and stability of the devices.^[13,14] Commonly, metal oxides including titanium dioxide (TiO_2), tin oxide (SnO_2), and zinc oxide (ZnO) have been used as the ETL in PSCs. Organic material including spiro-OMeTAD (2,2'7,7'-Tetrakis[N,N-di(4-methoxyphenyl)

amino]-9,9'-spirobifluorene), PTAA (poly-[bi(4-phenyl)] (2,4,3-trimethylphenylamine)), and polymer PEDOT:PSS (poly (3,4-ethylenedioxythiophene): polystyrene sulfonate) and inorganic materials such as copper iodide (CuI), nickel oxide (NiO), copper(I) thiocyanate ($CuSCN$), copper indium gallium (di)selenide (CIGS), and copper oxide (CuO) have been employed as an HTL.^[15–18] However, our primary focus lies in the coating process of the perovskite absorber layer rather than ETLs and HTLs.

A. Khorasani
Department of Electrical-Electronics Engineering
Abdullah Gül University
Kayseri 38080, Turkey
E-mail: azam.khorasani@agu.edu.tr

 The ORCID identification number(s) for the author(s) of this article can be found under <https://doi.org/10.1002/aesr.202300275>.

© 2024 The Authors. Advanced Energy and Sustainability Research published by Wiley-VCH GmbH. This is an open access article under the terms of the Creative Commons Attribution License, which permits use, distribution and reproduction in any medium, provided the original work is properly cited.

DOI: [10.1002/aesr.202300275](https://doi.org/10.1002/aesr.202300275)

F. Mohamadkhani
Department of Materials science and engineering, school of engineering,
Shiraz university
Shiraz 7134851154, Iran

M. Marandi
Physics Department
Faculty of Science
Arak University
Arak 38156, Iran

H. Luo, M. Abdi-Jalebi
Institute for Materials Discovery
University College London
Malet Place, London WC1E 7JE, UK
E-mail: m.jalebi@ucl.ac.uk

The deposition of the perovskite absorber layer is crucial for achieving high performance in PSCs. Different deposition methods have been utilized for the fabrication of various structures of high-performance hybrid organic–inorganic PSCs.^[19–22] Commonly, the solution-based spin-coating method has been used in lab-scale PSCs with great performance. Accordingly, with increasing energy crisis, enormous efforts have been made for commercialization and mass production of competitive and economic perovskite photovoltaics. Owing to poor stability and scalability challenges, deep gaps exist for industrial application and market entry of perovskite technology. The main challenges for large-area PSCs are the uniformity and controlling perovskite morphology, which depend on deposition technique. On the other hand, nonuniform absorber layers have intensified the instability problem under moisture invasion.^[23] Additionally, surface defects and incomplete coverage of perovskite film impose leakage paths, inefficient light harvesting, and as a result lower filling factor and weak performance of solar cells. Furthermore, cheap and effective scalable deposition techniques are crucial parts for commercializing of PSCs. The most common used deposition methods for scalable fabrication of PSCs can be divided into physical deposition techniques like thermal evaporation and chemical deposition techniques, like spin coating, screen printing, gravure printing, slot die coating, inkjet printing (IJP), and doctor blading.^[8–12,24–27]

Generally, one-step and two-step coating processes have been utilized in the various deposition techniques of perovskite layers. The one-step process involves applying a solution containing both organic and inorganic perovskite compounds onto a substrate to coat a perovskite film. In the two-step process, a layer of lead iodide (PbI_2) is first deposited onto the substrate, followed by the application and annealing of the methylammonium iodide ($\text{CH}_3\text{NH}_3\text{I}$ –MAI) solution to create methylammonium lead triiodide (MAPbI_3) perovskite. Poor morphologies with imperfections and incomplete surface coverage typically have been created via simple solution-processed deposition technology. However, achieving high uniformity, lower defect density, and fewer pinholes over a large area of perovskite is crucial for creating more stable PSCs.^[28] The irreproducible spin-coating technique used in research labs, which results in the wastage of more solutions and uneven coverage, is unsuitable for depositing large-area PSCs.^[29] Throughout the spin-coating process, a consistent centrifugal force is applied to the perovskite solution, and its speed significantly impacts the thickness and structure of the perovskite layer in the spatial distribution, presenting a challenge for scalable deposition methods. It is important to have a uniform perovskite layer throughout the solar cell to ensure its efficiency and stability. To commercialize PSCs, it is essential to achieve a consistent and reproducible layer thickness across large-area substrates.

In addition to applicable coating techniques for long-term stable devices, upscaling design is crucial for high-efficiency solar cells. Reducing dead area, adapting to flexible substrates, and integrating architecture play crucial roles in scaling up single cells into large and efficient modules, efficiently.^[30] Commonly, PSCs have been fabricated on the transparent conductive oxides (TCO) with sheet resistance of $\approx 10 \Omega \text{ sq}^{-1}$.^[31] Unfortunately, the sheet resistance of TCO increases at large scales, resulting in

enhanced current losses in the solar cell.^[28] Additionally, the creation of pinhole-free and nondefect perovskite layer is fragile in large area.^[32] To optimize these challenges, a substrate is usually divided into smaller subcells; hence, series and parallel connections have been designed for large-area PSCs. The most efficient way to achieve high-power output is through series connection, rather than parallel connection. Series connections can achieve high open-circuit voltage (V_{OC}) but relatively low current output, while parallel connections produce high current density and lower V_{OC} .

Typical perovskite solar modules are individual cells which are serially interconnected on the same substrate, as a monolithic integration. Monolithic interconnection is a complementary option for reducing defects in perovskite thin film for fabrication of perovskite solar modules. Mainly, in module design, narrow interconnection zones reduce dead area and in consequence lead to best performance in solar modules. Nonhomogeneous and wide interconnection zones result in higher resistance for the charge traveling from subcells to another. Moreover, smoothness and homogeneity of interconnection zones enable us to fabricate better modules without heat damage or surface roughness.

The mass production of PSCs has been hindered by the degradation of perovskite under temperature, humidity, light, and oxygen, as well as the challenge of achieving coating uniformity and pinhole-free perovskite thin films with high stability and reproducibility. The quality of the perovskite layer plays a crucial role in charge transportation and recombination, necessitating the creation of a pinhole-free full-coverage perovskite film for highly efficient PSCs. Several strategies, such as precursor engineering,^[33–35] solvent selection,^[36,37] additives,^[20,38] deposition methods,^[39,40] and annealing processes,^[41,42] have been employed to obtain a compact and uniform perovskite layer with large crystal domains. Various analytical techniques, including scanning electron microscopy (SEM), X-ray diffraction (XRD), atomic force microscopy (AFM), time-resolved photoluminescence (TRPL) measurement, energy-dispersive X-ray spectroscopy (EDS), UV-vis absorption, transmittance, and steady-state photoluminescence (PL) measurement, have been utilized to characterize perovskite films.

Numerous studies have been conducted to overcome barriers in fabricating highly efficient and stable solar cells. These deposition techniques show promise in achieving higher efficiencies and stability through easily accessible and, in some cases, low-temperature approaches. However, the application of these various technologies to scale up PSCs into modules and achieve commercialized levels of perovskite photovoltaics is still uncommon.

The review provides a summary of various deposition techniques for upscaling perovskite thin films in photovoltaic applications. It focuses on film quality and device performance, examining the benefits and challenges of each technique as shown in **Figure 1**. Outstanding perovskite deposition methods play a key role in manufacturing high-efficiency and stable PSCs. To scale up film production, various deposition techniques have been explored. Furthermore, the application of these techniques in PSC module fabrication is also discussed. The objective of this review is to provide a comprehensive overview of these techniques, focusing on film quality and device performance.

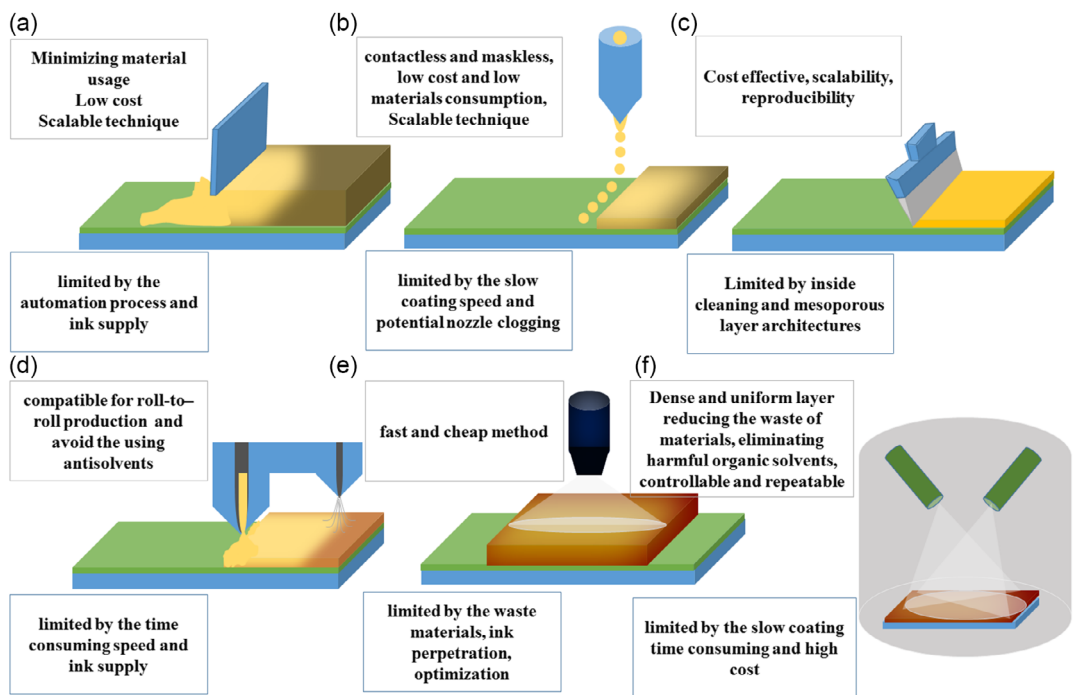


Figure 1. a) Schematic diagrams of blade coating, b) IJP, c) screen printing, d) slot-die coating, e) spray coating, and f) PVD techniques.

2. Blade-Coating Technique

Blade-coating technique has been widely used for the deposition of large-area thin films. In the blade-coating process, the precursor solution is directly loaded onto the substrate and then spread on the surface by a knife-type coater. The utilized blade (Meier bar) must continuously move on the solution/substrate to form a uniform film; it is an appropriate technique for roll-to-roll coating methods and mass production. Researchers seek to manipulate material compositions, solvent engineering, device structure, and fabrication process to achieve high efficiencies. The nucleation and growth of perovskite crystallites have a significant impact on solar module performance. Fast nucleation and slow growth production result in a perovskite film with larger grain sizes. Techniques such as heat treatment, additive utilization, addition of an antisolvent, gas quenching, or rapid solvent removal by vacuum can lead to rapid nucleation and gradual growth, consequently resulting in larger grain sizes of the perovskite layer.

Some researchers have been reporting the use of various ETLs or HTLs to improve blade-coated PSCs. In 2015, Wang's group achieved an efficiency of 14.9% with C_xTiO₂/ZrO₂/NiO/carbon(MAPbI₃) structure by the blade-coating process.^[43] They utilized NiO as an inorganic HTL in PSCs with carbon electrodes. The hole extraction NiO interlayer blocked the electron pathway and enhanced the difference between electron and hole Fermi levels, thereby improving the device V_{OC} . The blade-coating process applied by Wang's group has demonstrated the potential for scalability and cost-effectiveness in the fabrication of PSCs.

During the blade-coating process, the solution's flow often leads to defects and pinholes in the perovskite film. The island structure of the blade-coated perovskite film forms due to differing surface energies between the perovskite solution and the substrate.^[44] Achieving full substrate coverage with the perovskite solution is a challenge when aiming for a defect-free perovskite layer. The solution's wettability plays a crucial role in substrate coverage and is influenced by the solvent of the perovskite ink. Additionally, rapid crystallization at low temperatures during blade coating results in small grains, low crystallinity, and a high defect density in perovskite films. Common solvents for perovskite ink production, such as DMSO and DMF, have high solubility for perovskite precursors. However, they are not suitable for quickly depositing a compact and smooth blade-coated perovskite film at room temperature. To enhance the quality of perovskite film, it is suggested to either mix the solvents or utilize solvent engineering techniques.^[28] This can help to improve the film's morphology and enhance its electronic properties, ultimately leading to better performance in perovskite-based devices. Mixing solvents can optimize the crystallization process, while solvent engineering techniques can control the nucleation and growth of perovskite crystals, resulting in a more uniform and defect-free film. N,N-Dimethylformamide (DMF) is usually used as a solvent in perovskite solutions, which is toxic and should be replaced with nonhazardous materials. The mixture of γ -butyrolactone (GBL) and dimethyl sulfoxide (DMSO) is a suitable candidate as the perovskite solvent.^[40,45] Huang et al. demonstrated that the blending ratio of 9:1 by volume of DMSO and GBL resulted in higher-quality perovskite films with larger crystalline domains. Additionally, the surface of the blade-coated

perovskite film became smoother with the addition of polyethylene glycol (PEG) to the perovskite precursor. They finally obtained the highest PCE of 17.02% on an active area of 0.09 cm^2 in ambient conditions.^[37] While the output efficiency of subsequent solar cells may not be as high as when using toxic solvents, the sustainability of the solar cell manufacturing processes, environmental impacts, and the removal of toxic precursor materials are crucial factors for the commercialization of ecofriendly perovskite photovoltaic devices.

The structural properties of blade-coated perovskite layers are significantly affected by the rate of drying. The solidification or evaporation rate of the solvent can be accelerated with a heat treatment process. Zhong et al. studied the changes in the behavior of solidifying perovskite films *in situ* with an increase in the coating temperature from 50 to 150 °C.^[46] Three solvate phases were observed in this study for equimolar MAI and PbI₂ in DMF, along with MAI-rich and PbI₂-rich crystalline solvates. At low temperatures of 25–50 °C, the solidification process occurs at $\approx 47\text{ s}$.

In this temperature range, the solidification rate is quite low and forms a DMF-solvated lead iodide (PbI₂)-rich film while the perovskite phase is absent. The solvent evaporation rate was much faster at 80 and 135 °C, it occurs only after ≈ 13.4 and $\approx 2.4\text{ s}$, respectively. At intermediate temperatures of 50–80 °C, an equimolar MAPbI₃-DMF solvated phase incorporating increasingly more methylammonium iodide ($\text{CH}_3\text{NH}_3\text{I}/\text{MAI}$) is formed. The excessive coordination of lead and DMF at the exclusion of MAI is circumvented due to rapid loss of the solvent at elevated temperature ($>100\text{ }^\circ\text{C}$). In this condition, the disordered sol-gel state collapses into an equimolar crystalline solvated phase, which is rather a PbI₂-rich solvate. At 135 °C, the solidification rate is high enough to prevent the formation of the PbI₂-rich phase and cause the direct conversion of precursors to perovskite phase. The schematics of perovskite film formation in different regimes and corresponding SEM images are shown in Figure 2. At intermediate temperatures between 80 and 100 °C, a combination of ribbon-like and compact morphologies

is observed compared to the PbI₂ phase with ribbon-like morphology. At temperatures above 100 °C, the perovskite crystals nucleate and grow directly in the colloidal ink. These processes produce films with compact structure and minimal solvent retention. The presence of the PbI₂ phase results in reduced device performance. However, temperatures above 135 °C prevent the formation of the solvate or PbI₂ phase. Hence, the colloidal sol-gel precursor can directly convert into MAPbI₃. Ultimately, this group achieved a champion performance of 17.54% PCE at a temperature of 150 °C.

The crystallinity of the blade-coated perovskite layer can be affected by additives, as well. The grain sizes of perovskite layer were increased from 50 to 200 nm by 0.5% mol Pb(SCN)₂ with respect to the perovskite concentration. Ernst et al. fabricated the blade-coated modules with a stabilized efficiency of 12.6% with an aperture area of 66 cm^2 , in comparison with 18.1% on a small-area spin-coated device using FA_{0.83}Cs_{0.17}PbI₃ perovskite precursor solution (with 1 mol% Pb(SCN)₂ as an additive).^[47]

As mentioned before, mainly perovskite is deposited in two methods, one-step and two-step or sequential deposition method. In two-step route of perovskite deposition, first PbI₂ solution was blade coated on the substrate, followed by coating MAI solution and annealing the wet film to fabricate MAPbI₃ perovskite layer. The main challenge in this coating process is that PbI₂ film is unstable and incompletely converts to the crystallized perovskite layer. Several studies are reported to solve this problem. For example, Matteocci et al. added a small amount of MAI to PbI₂ (M-PbI₂) precursor, which increases the nuclei density during crystal growth, leading to the formation of cuboid crystals with a higher absorbance coefficient.^[48] They achieved a PCE of 14.7% with an aperture area of 47 cm^2 with air jet-assisted blade coating of PbI₂ layer.

The additives can assist in the crystallization of the perovskite film in a two-step deposition method. The use of additives can also improve the film's morphology and enhance its stability, making it more suitable for use in various electronic and optoelectronic devices. Huang et al. observed that MAI associated

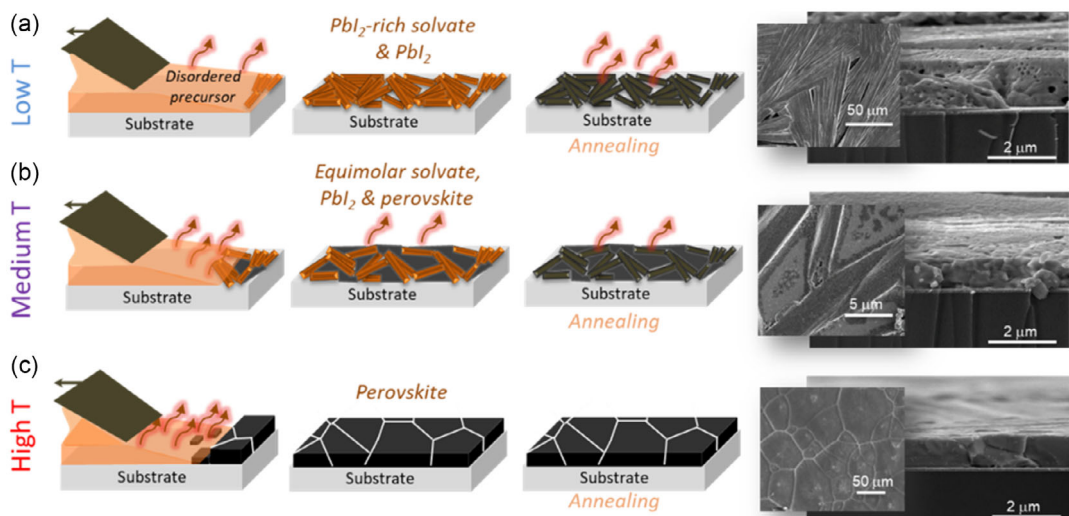


Figure 2. Schematic representation and SEM images of blade-coated perovskite film formation at a) low ($\approx 25\text{--}50\text{ }^\circ\text{C}$), b) intermediate ($\approx 80\text{ }^\circ\text{C}$), and c) high ($>100\text{ }^\circ\text{C}$) temperatures. Reproduced with permission.^[46] Copyright 2018, ACS Eneg Letters, ACS.

with polyurethane (PU) added in PbI_2 (MP-PbI_2) precursor forms an intermediate complex ($\text{MAI-PbI}_2\text{-PU}$) with an oriented crystal structure, resulting in a compact perovskite thin film with fewer pinholes.^[39] Glancing incident X-ray diffraction (GIXRD) patterns were used to analyze the evolution of PbI_2 films deposited from different precursor inks. Figure 3a shows that all PbI_2 films exhibit a prominent diffraction peak at 12.7° , which corresponds to the 001 lattice plane of crystallized PbI_2 . Furthermore, the pristine PbI_2 film shows a distinct diffraction peak at 9.6° . It has been indicated that a complex of PbI_2 and dimethyl sulfoxide (DMSO) formed. To convert PbI_2 to perovskite, a blade-coated MAI solution was used; following the deposition process, the sample underwent thermal annealing at 100°C for 10 min. Figure 3b displays the GIXRD patterns of perovskite films made from each PbI_2 precursor ink. The diffraction peaks located at 14.2 , 28.5 , and 31.9° correspond to the 110 , 220 , and 310 lattice planes of $\text{CH}_3\text{NH}_3\text{PbI}_3$ perovskite, respectively. The synergistic impact of trace MAI and PU enhances these peaks. Additionally, the standard diffraction peak intensity of PbI_2 decreases significantly, indicating complete conversion from the intermediate complex to the perovskite crystal. Using $\text{MAI-PbI}_2\text{-PU}$ precursor ink in the blade-coated planar p-i-n PSCs exhibits PCE up to 19.01% with an aperture area of 0.12 cm^2 and PCE of 11.07% on an active area of 25 cm^2 solar modules.

Another research for solving the problem of incomplete conversion of the compact PbI_2 layer to perovskite film was done using a two-step method. Zhang et al. found a nonvolatile solvent like 4-tert-butylpyridine (TBP) that has low solubility with PbI_2 and assists in forming a nanoporous PbI_2 film.^[40] The removal of the additive solvent leaves the pores in the PbI_2 films, which helps in better penetration of MAI to PbI_2 layer. However, the large amount of the solvent leads to the formation of too large pores and undesired porous structure in the perovskite films. Figure 3c indicates the diagram of the perovskite converted from pristine PbI_2 films and perovskite seed-assisted porous PbI_2 films, respectively. The high PCEs of 16.54% and 13.32% were achieved for 5×5 and $10 \times 10\text{ cm}^2$ perovskite solar modules, respectively.

In one-step deposition, a stoichiometric solution including both organic and inorganic contents is cast onto a substrate. Afterward, the resulting film is annealed on a hot plate to obtain the perovskite phase. Antisolvent is drop cast on the film or additives are used in order to control the solidification and crystallization.^[49,50] Addition of thiourea (TU) can effectively improve the permeation of perovskite precursor solution into the mesoporous scaffold, leading to the formation of more ordered and well-defined perovskite crystals.^[51] Thiourea enables deposition of the high-quality dense perovskite film with uniform and large crystalline size.^[52] The schematic of how thiourea influences the growth of perovskite crystals is illustrated in Figure 3d. Thiourea can create hydrogen bonds with the perovskite crystals or Lewis acid–base adducts to retard their growth. Essentially, a strong coordination is established between thiourea and PbI_2 , which proves effective at grain boundaries. Wang et al. utilized the Lewis base thiourea (TU) into the perovskite precursor in one-step deposition method for constructing flexible solar devices.^[52] Figure 3e–j shows the top-view SEM images of perovskite film deposited on flexible polyethylene naphthalate/indium tin

oxide (PEN/ITO) substrates and on rigid glass/ITO substrates, with varying molar ratios of TU. By adding TU, the dense and large crystal grains were obviously obtained. However, at 7% and 10% amount of TU, diameters of crystals grains enlarged over $1\text{ }\mu\text{m}$, and visible holes were generated in the film. Finally, optimized PCE up to 19.41% and filling factor exceeding 80% were obtained with the incorporation of 5% TU, for flexible perovskite cells on a low-cost plastic substrate.

Li et al. fabricated high-quality mirror-like monoammonium zinc porphyrin (ZnP)-doped perovskite film on fluorine-doped tin oxide (FTO) with an area of 16 cm^2 by blade coating.^[35] ZnP binds to the surface of the perovskite crystal and prevents the cations from escaping, effectively reducing the formation of defects through molecular encapsulation. Efficient crystallization control of the perovskite film led to achieving efficiency as high as 18.3% on active area of 1.96 cm^2 .

As discussed earlier, interface engineering and defect passivation in PSCs are vital to obtain the maximum performance. In solution deposition, the surface of perovskite film is full of imperfections such as defects, trap-state Pb–I antisites (PbI^{3-}), metallic Pb clusters, MA ion, and undercoordinated halide and Pb ions defects which can act as nonradiative charge recombination sites and significantly influence the performance of the device.^[53–55] Qiu et al. used a cost-effective and ecofriendly biomaterial ploy-L-lysine (PLL) as an additive to passivate the defects of blade-coated perovskite film.^[38] A simple and effective strategy to decrease perovskite surface defects is the usage of functional polymers as a surface passivator. Particularly, hydrophobic polymers on surface PSCs can serve as a moisture barrier layer, which helps to reduce cell deterioration. PLL polymers with many $-\text{COO}^-$ anions and $-\text{NH}^{2+}$ cations enable to chelate the undercoordinated Pb^{2+} and suppress the formation of metallic Pb which will otherwise form trap states. They found that the device with PLL additive delivered the PCE of 19.45% with V_{OC} of 1.1 V , which is nearly 100 mV higher than the control device.

In 2021, Castro-Hermosa et al. fabricated fully printed inverted PSCs, except for electrodes, by the blade-coating technique.^[56] They incorporated the nanometer-thick bathocuproine (BCP) hole-blocking buffer layer in PSCs at a relative humidity up to 50% . The charge accumulation and recombination reduced at the PCBM/Ag interface with blade-coated BCP layer. The fully printed PSCs yield the maximum efficiency of 14.9% on an aperture area of 0.5 cm^2 . Yang and co-workers demonstrated a fully scalable deposition scheme for perovskite module fabrication. They utilized spray-coated TiO_2 ETL and blade coated both a perovskite absorber layer and a spiro-OMeTAD-based HTL.^[57] The results indicated that the performance of perovskite modules is critically affected by the thickness of TiO_2 ETL film. The monolithic interconnection contact (FTO/ TiO_2 /Au) in modules leads to different impacts of ETL thicknesses on modules and small-area cells, which are absent in small-area cells. Ultimately, after optimizing the behavior of the interconnection junction, perovskite composition, and blade coating HTL, a stabilized PCE of 15.6% was achieved for a four-cell $\text{MA}_{0.7}\text{FA}_{0.3}\text{PbI}_3$ perovskite module with an aperture area of $\approx 10.36\text{ cm}^2$.

As mentioned, the series resistance of TCO increases in large-area devices. Thus, redesigning of perovskite solar modules has been applied to reduce its effect when scaling up devices, and

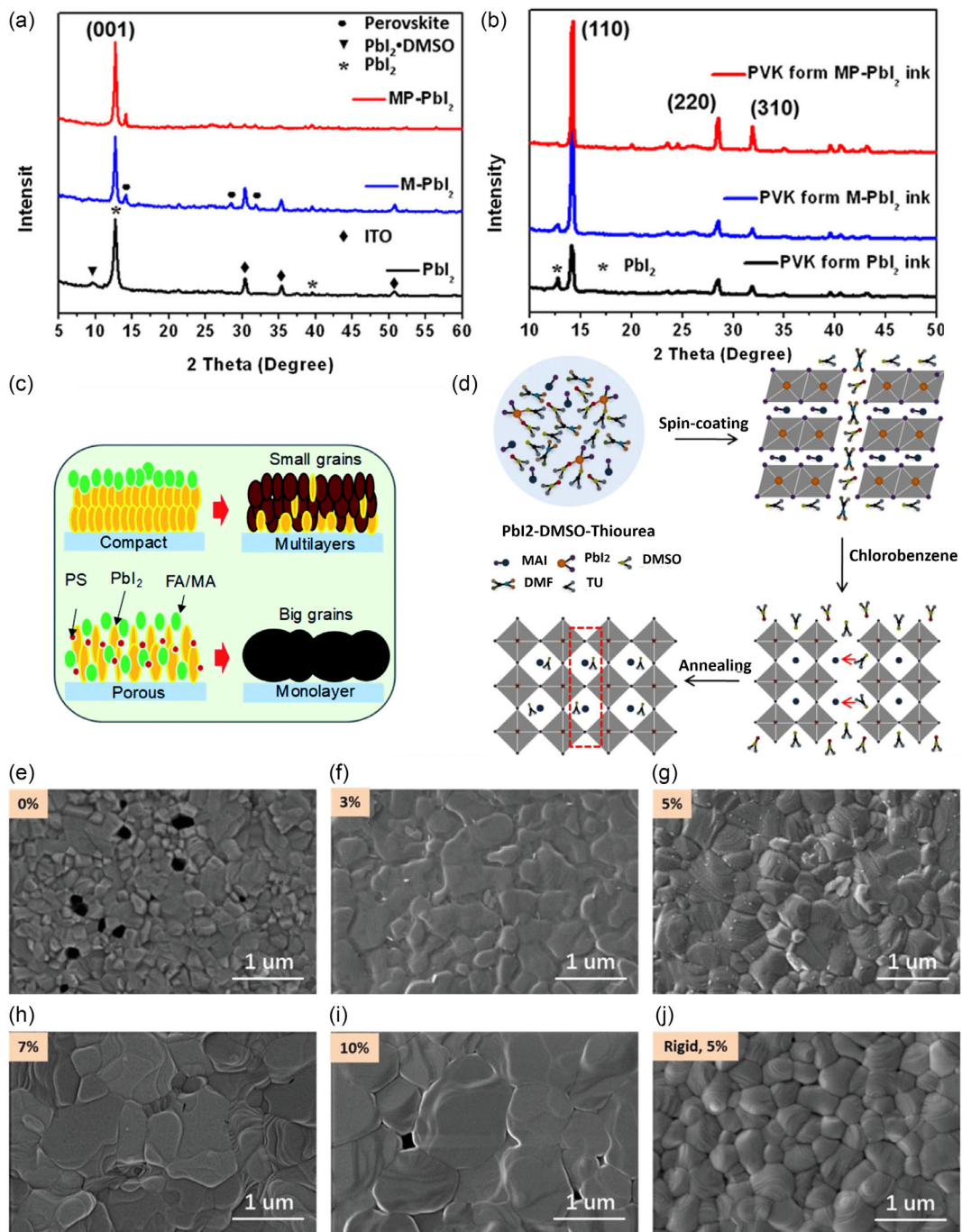


Figure 3. GIXRD patterns: a) pristine PbI_2 , M-PbI_2 , and MP-PbI_2 inks. b) $\text{CH}_3\text{NH}_3\text{PbI}_3$ perovskite films converted from pristine PbI_2 films and M-PbI_2 , and MP-PbI_2 films, respectively. Reproduced with permission.^[39] Copyright 2020, Journal of Physical Chemistry C, ACS. c) Diagram of perovskite converted from pristine PbI_2 films and perovskite seed-assisted porous PbI_2 films, respectively. Reproduced with permission.^[40] Copyright 2015, Journal of Materials Chemistry A, RSC. d) Schematic illustration explaining how thiourea affects the growth of perovskite crystals. During the annealing process, DMSO easily evaporates from the PbI_2 framework, and the combination of thiourea with PbI_2 in the films slows down the reaction between PbI_2 and MAI, resulting in larger perovskite grains.^[51] Copyright 2018, Solar RRL, Wiley. e–j) SEM images of perovskite films processed with varying amounts of TU-level blade on PEN/ITO and glass/ITO flexible and rigid substrates, respectively. Reproduced with permission.^[52] Copyright 2020, Advanced Functional Materials, Wiley.

rapid crystallization at low temperature results in small grains, low crystallinity, and high defect density in perovskite films during blade coating.^[58] In 2019, Hung's group reconciled fast and safe deposition with large grains and high crystallinity of the perovskite layer by engineering a new ink design.^[58] Even though common solvents such as DMSO and DMF have high solubility for perovskite precursors, they are not suitable for rapid, smooth, and compact perovskite film deposition at room temperature using the blade method. Highly volatile solvents such as 2-methoxyethanol (2-ME) and acetonitrile (ACN), due to rapid evaporation during fast deposition, result in perovskite films with low crystallinity and poor contact with the substrates. To improve perovskite crystallinity, a combination of the two solvents was used in a certain ratio. Using a combination of these two solvents in a certain ratio allowed for a slow release from the as-coated film, which provided enough time for the perovskite grains to grow into large sizes with high crystallinity and good contact with the substrate. Perovskite modules with a PCE of 16.4% and an aperture area of 63.7 cm² were achieved by uniformly blade coating perovskite films at a speed of 99 mm s⁻¹ at room temperature.

In the roll-to-roll manufacturing process of perovskite modules, flexible substrate plays an important role. Corning Willow glass is a moisture barrier that simplifies the encapsulation procedure and is compatible with the high-throughput roll-to-roll process. The efficient flexible perovskite solar module with blade-coating technique was demonstrated by Dai and co-workers in 2020.^[59] High-quality perovskite films on flexible Corning Willow glass were obtained using additive engineering. Ammonium chloride (NH₄Cl) was added in precursor solution to retard perovskite nucleation and as a result, improve morphology and passivation of perovskite film. In addition, Willow glass is a moisture barrier that simplifies encapsulation procedure and is compatible with the high-throughput roll-to-roll process. Finally, the efficiency of a flexible perovskite module approached 16.0% for aperture area of 42.9 cm². In 2021, Seok's group reported that air knife-assisted bar coating can be used to deposit dense and uniform perovskite films.^[60] Two different chemicals, 2- methoxyethanol as a solvent and n-cyclohexyl-2-pyrrolidone as an additive, were used to create high-efficiency and large-area perovskite mini-modules. Due to the additive, a balance between rapid nucleation and slowed crystal growth in the precursor solution improved the uniformity of perovskite.

Deposition process of the perovskite film is a major part of fabrication for highly efficient solar cells compared to other functional layers. Hence, nucleation and growth of perovskite crystallites are critical, and fast nucleation and slow growth produce perovskite film with larger grain sizes. Heat treatment, utilizing additive, addition of an antisolvent, gas quenching, or generally quick removal of solvents by vacuum lead to rapid nucleation and gradual growth and as a consequence larger grain sizes of perovskite layer.^[60–71]

In summary, the comparison of the published blade-coating technique in PSCs and modules is tabulated in Table 1. Here, we can conclude that the blade-coating technique with minimized materials waste is a low-cost approach for fabricating large-scale PSCs, in which one-step and two-step deposition technique could be used in this method. The intermediate phase film is critical for the compact and pinhole-free perovskite absorber

layer. Temperature and additives have an essential effect on the morphology and structure of perovskite film, as well as stability and efficiency of PSCs. Although it is a simple and cost-effective technique, it is restricted to the automation process and ink supply.

3. The Inkjet Printing Technique

Various printing techniques including gravure, screen, flexography, and inkjet have been used to deposit different materials on various substrates.^[72–74] In recent years, IJP with easily changeable digital print patterns has been utilized for coating micro- and nanolayers on various wide substrates.^[75] The IJP technique is an effective and promising method in photovoltaic technology which has been considered with significant advantages such as contactless and maskless. On the other hand, various multilayers with different shapes can be deposited by this technique. Moreover, the IJP is a streamlined technique with low cost and low materials consumption.

Hence, IJP method is suitable in scalable fabrication techniques for all types of PSC devices, such as n-i-p and inverted p-i-n architectures.^[76] The inkjet-printed technique developed a uniform perovskite thin film with a columnar crystal structure and free of horizontal grain boundaries throughout its entire thickness.^[77] As mentioned, this method is applicable for large areas, the roll-to-roll process, and fabricates flexible solar cells. In the IJP technique, ink in the nozzle is dropped on a substrate; the common transfer methods are classified as continuous IJP and drop-on-demand IJP.^[78] Figure 4a displays the schematic continuous drop ejection from the printhead for continuous inkjet technology. These drops are charged while passing through an electric field, and then deflection plates divert the charged droplets to the substrate. The extra ink that is not needed is collected by gutter and recirculated back to the reservoir. Despite the continuous IJP technique, in drop-on-demand technology, droplets are ejected from the nozzle only when required. Consequently, this dripping technique has benefits like noncontact printing, the use of small amounts of materials, mask-free designs, and cost-effectiveness.

The schematic diagram for the drop-on-demand IJP is also shown in Figure 4b. In general, in drop-on-demand method, the drops are formed by the creation of a pressure pulse within the printhead. The common mechanisms for generating this pressure are "thermal" and "piezoelectric," which are shown in Figure 4c,d. The process of creating high-performance IJP perovskite thin films involves three main steps, as shown in Figure 4e. First, ink preparation. The perovskite precursor solution is formulated with a solvent system to produce a printable ink. Second, drop-on-demand IJP process. A waveform is used to control the ejection of individual ink droplets from a piezoelectric transducer. The printed droplets on the substrate merge to form a wet film. The amounts of ink deposited and layer thickness are determined by the printed resolution. Third, drying and annealing. The printed TCP wet film is transferred to a vacuum chamber to accelerate the evaporation of solvents and promote nucleation of the perovskite thin film. The crystallization of the perovskite thin film begins, and the chamber is then vented. The perovskite crystallization is completed in

Table 1. A comparison of the published blade-coating technique in PSCs and modules.

Structure	PCE [%]	V _{OC} [V]	Active area [cm ²]	Coating methods for different layers	Coating process of perovskite film	References
ITO/PEDOT:PSS/1,8-diiodooctane: MAPbI _{3-x} Cl _x /PCBM/C60-bis/Ag	9.29	0.92	0.031	Spin coating/blade coating/spin coating/thermal evaporation	One step using precursor solution with 1,8-diiodooctane additive	[33]
ITO/PTAA/1,3-diaminopropane-MAPbI ₃ /PC ₆₀ BM/Cu	20	1.14	1.1	Blade coating/blade coating/thermal evaporation/thermal evaporation	One step anchoring bilateral alkyl amine additives	[34]
FTO/PEDOT:PSS/MAPbI ₃ /C ₆₀ /BCP/Ag	13.03	5.41	10.56	Spin coating/blade coating/thermal evaporation	One-step method using TABC* process	[36]
FTO/TiO ₂ /MAPbI ₃ /spiro-OMeTAD/Au	17.55	1.05	0.16			
FTO/NiO _x /MAPbI ₃ /PCBM/PEI/Ag	17.02	1.09	0.09	Spin coating/blade coating/spin coating/thermal evaporation	One step controlling the morphology of perovskite using green solvent	[37]
ITO/PTAA/ploy-L-lysine: MAPbI ₃ /BCP/PCBM/Ag	19.45	1.11	0.09	Spin coating/blade coating/spin coating/thermal evaporation	One step using ploy-L-lysine to passivate defects of perovskite film	[38]
FTO/SnO ₂ /MA _{0.7} FA _{0.3} PbI ₃ /spiro-OMeTAD/Au	13.32	11.826	53.64	Spin coating/blade coating/spin coating/thermal evaporation	Two steps using 4-tert-butylpyridine (TBP) to produce porous PbI ₂ film	[40]
	16.54	6.71	10			
	20.49	1.09	0.16			
ITO/PTAA/FA _{0.4} MA _{0.6} PbI ₃ /ICBA/C ₆₀ /BCP/Cu	18.3	1.03	Not mentioned	Spin coating/blade coating/spin coating/thermal evaporation	One step tuning the absorption onset by perovskite composition	[44]
FTO/TiO ₂ /MAPbI ₃ /spiro-OMeTAD/Au	17.06	1.08	1	Chemical bath deposition/blade coating/spin coating/thermal evaporation	One step study the phase transition in blade and spin coating of perovskite	[45]
	18.74	1.07	0.09			
ITO/MeO- 2PACz/Pb(SCN) ₂ ; FA _{0.83} Cs _{0.17} PbI ₃ /PCBM/BCP/Al	16.2	0.99	1.1	blade coating/blade coating/blade coating/thermal evaporation	One step by the addition of lead(II) thiocyanate (Pb(SCN))	[47]
PEN/ITO/PEDOT:PSS/PTAA/thiourea: MAPbI ₃ /PCBM/BCP/Ag	16.61	1.1	1	Spin coating/blade coating/spin coating/thermal evaporation	One step using thiourea to modulate the crystal growth	[52]
	17.29					
FTO/TiO ₂ /MA _{0.7} FA _{0.3} PbI ₃ /spiro-OMeTAD/Au; four cell module	15.6	4.35	10.36	Spray pyrolysis/blade coating/blade coating /thermal evaporation	One-step ETL thickness optimization by spray coating	[57]
FTO/TiO ₂ /MA _{0.7} FA _{0.3} PbI ₃ /spiro-OMeTAD/Au; cell	17.9	1.09	0.12			
MgF ₂ /glass/ITO/PTAA/MAPbI ₃ /C ₆₀ /BCP/Cu	19.72	1.09	10.36	blade coating/blade coating/thermal evaporation	One step adding NH ₄ Cl into perovskite precursor to prevent void formation	[59]
	15.86	13.142	42.9			
FTO/TiO ₂ /FA _{0.95} MA _{0.05} I _{2.85} Br _{0.15} /spiro-OMeTAD/Au	20.99	5.79	15	Spin coating/blade coating/spin coating/thermal evaporation	One step formation of a uniform film by addition of 2methoxyethanol to perovskite precursor	[60]
FTO/TiO ₂ /MA _{0.7} FA _{0.3} PbI ₃ /spiro-OMeTAD/Au	15.6	4.38	10.36	Spray pyrolysis/blade coating/blade coating/thermal evaporation	One step using NMP/DMF as solvent to optimize TiO ₂ thickness	[61]
FTO/SnO ₂ /Cs _{0.05} (MA _{0.17} FA _{0.83}) _{0.95} Pb(I _{0.83} Br _{0.17}) ₃ /PEAI/spiro-OMeTAD/Au	16.13	18.15	0.5	Blade coating/hybrid blade, slot-die coating/slot die coating thermal evaporation	Two-step method using hybrid blade, slot-die coating technique	[62]
ITO/PEDOT:PSS/MAPbI ₃ /PCBM/BCP/Ag	13.1	1.01	0.5	All-roll-to-roll blade coating	One step with focus on the BCP deposition method	[63]
FTO/SnO ₂ PbO/MAPbI ₃ /spiro-OMeTAD/Au	16.5	1.08	1	Spin coating/blade coating/spin coating/thermal evaporation	One step using DMF-free solvent for low-lighting indoor applications	[64]
ITO/PTAA/SAM/MeO-2PACz/MAPbI ₃ /C ₆₀ /BCP/Ag	14.64	1.073	1.008	Spin coating/spin coating/blade coating/thermal evaporation	One-step method	[65]
ITO/PTAA/Al ₂ O ₃ /MAPbI ₃ /PCBM/BCP/Ag	19.83	1.135	0.09	Spin coating/spin coating/blade coating/thermal evaporation	One step with 2-guanidinoacetic acid, l-aspartic acid, l-glutamic acid, and 3-guanidinopropanoic acid (3gpa), as passive agents	[66]

a final annealing step on a hot plate; therefore, nucleation and crystallization are completed in a pinhole-free perovskite thin film.

The first report on using inkjet-printed technique Copyright s in PSCs was reported by Wei et al. in 2014.^[79] They improved the efficiency from 8.51% to 11.60% by improving the interface

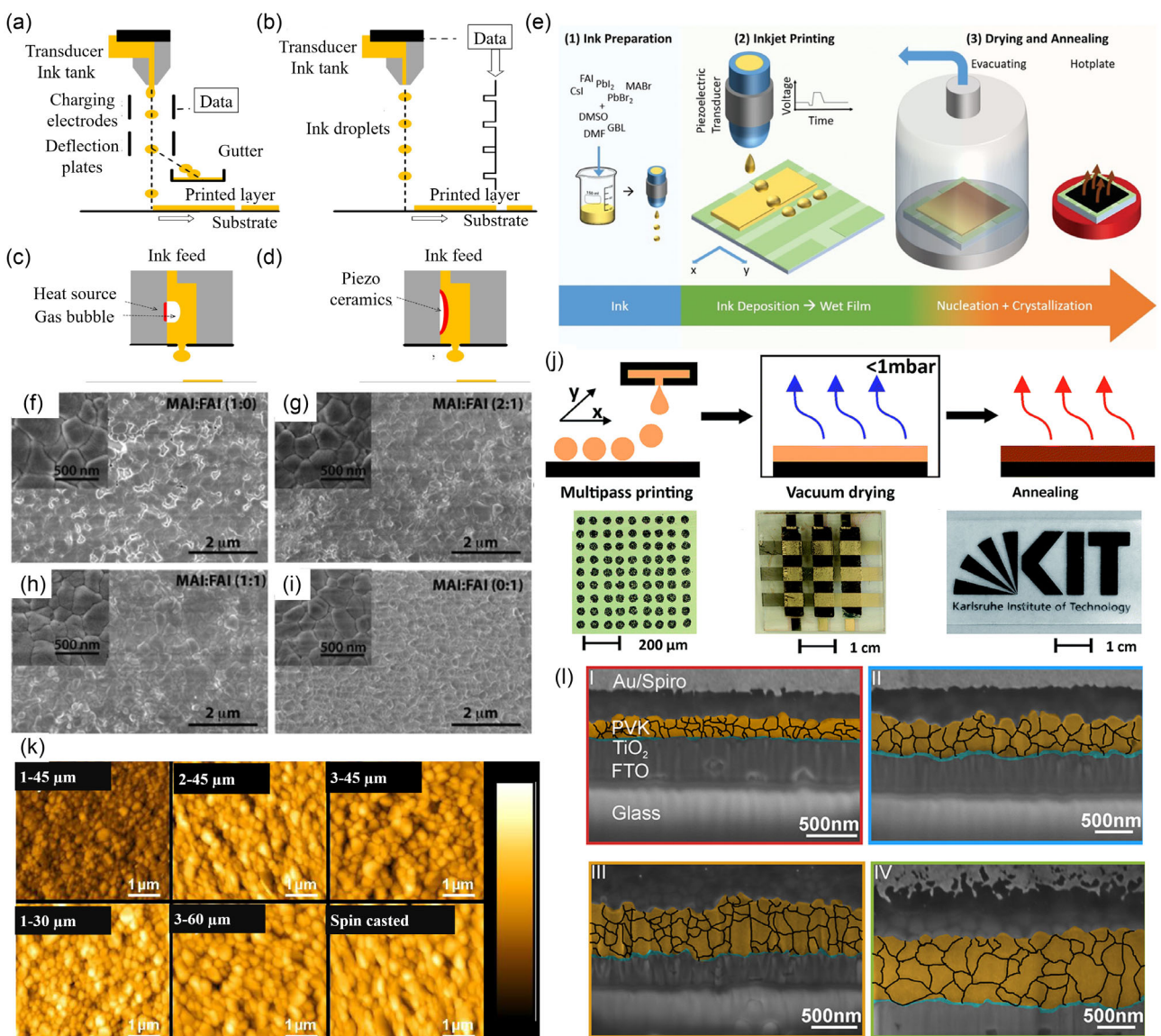


Figure 4. Schematic illustration of a) continuous-, b) drop-on-demand-, c) thermal-, and d) piezoelectric IJP, as described in another study.^[74,75,76] Copyright 2021, Woodhead Publishing, 2015, Wiley, 2010, Physics Report e) Schematic illustration of the main steps involved in IJP of triple-cation multicrystalline perovskite thin films. The steps include ink preparation, drop-on-demand IJP process, drying, and annealing. First, the ink is prepared. Then, the drop-on-demand IJP process is used to print the TCP wet film. The printed TCP wet film is then transferred to a vacuum chamber where the evaporation rate of the solvents is increased to induce nucleation of the perovskite thin film. The perovskite crystallization is initiated and the chamber is vented. Finally, the perovskite crystallization is completed in a final annealing step on a hot plate. Reproduced with permission.^[77] Copyright 2019, Advanced Energy Materials, Wiley. f-i) Top-view SEM images of perovskite layer fabricated by IJP with 1:0, 2:1, 1:1, and 0:1 MAI and FAI respectively on PbI₂-coated substrate at various ratios. Inset: Magnified SEM of the same substrate. Reproduced with permission.^[81] Copyright 2016, Materials Letters, Elsevier. j) Multipass printing for one-step MAPbI₃ ink, followed by an extra vacuum drying step to remove excess solvents and create a uniform perovskite layer. Reproduced with permission.^[84] Copyright 2016, Journal of Materials Chemistry A, RSC. k) AFM images of printed MAPbI₃ on FTO/TiO₂ substrates after annealing at 100 °C with various printing parameters, including the number of depositing processes and the dropping spacing and spin-cast reference. l) SEM images with variations in the thickness of the perovskite layer in IJP triple cation PSCs based on drop spacing. The thicknesses are as follows: I, 180 nm from 60 µm ds; II, 380 nm from 45 µm ds; III, 520 nm from 35 µm ds; and IV, 780 nm from 25 µm ds. The perovskite layer is marked in yellow, while the TiO₂ layer is marked in blue. However, the spiro-MeOTAD is partially damaged by the focused ion beam. Grain boundaries are outlined by a black line in another study.^[85] Copyright 2018, ACS Applied energy materials, ACS.

between $\text{CH}_3\text{NH}_3\text{PbI}_3$ and C electrodes through instant chemical transformation. This was achieved by implementing the C + $\text{CH}_3\text{NH}_3\text{I}$ ink formulation which creates an interpenetrating interface between $\text{CH}_3\text{NH}_3\text{PbI}_3$ and C electrodes, as opposed to using bare C. Consequently, lower charge recombination at the interface improves cell performance and efficiency. Li et al successfully deposited the perovskite $\text{CH}_3\text{NH}_3\text{PbI}_3$ layer on a mesoscopic TiO_2 film using the IJP technique in 2015 by incorporating nanocarbon as a hole extraction layer.^[80] Various amounts of methylammonium chloride ($\text{CH}_3\text{NH}_3\text{Cl}_3$, MACl) as a dopant and different temperatures were investigated in the printing solution as well. Heating the substrate and using additives have an impact on the morphology and structure of the printed perovskite films. As mentioned earlier, different additives decrease imperfections and trap states in the perovskite layer, resulting in a uniform film with high reproducibility. Particularly, nucleation and crystallization of the perovskite film will change with heating sublayers and using additives. The gradual change in the morphology of the perovskite film at the fixed table was observed at the temperature of 50 °C. Reduction of disc-like crystal plates, full surface coverage, and a continuous uniform perovskite layer were formed when \times increased to 0.6. High crystallization and improved interconnectedness of the perovskite film on the mesoporous (mp) TiO_2 led to achieving a PCE of 11.60%. In 2016, Bag et al. produced PSCs using a compatible roll-to-roll technique with a multichannel inkjet printer.^[81] Figure 4f-i demonstrates the formation of perovskite crystals from various compositions of MA to FA, showing the uniform formation of the perovskite layer through this method. The highest efficiency of 11.1% was achieved with a 2:1 MA to FA ratio.

Carbon-based PSC with high stability and reproducibility was fabricated by the IJP method by Hashemi et al in 2017. They achieved long-term stability for 1002 h under UV light illumination in air with the simple epoxy glue sealing of cells.^[82] Due to high durability, the carbon layer enables the use of easily accessible slow-drying, thick epoxy as the sealant for the cells. The epoxy without penetration into the pores of the printed carbon electrode or the photoactive area acts as a barrier against moisture and humidity intrusion. Jiang and co-workers reported a one-step method for aqueous-processed perovskite active layer via reactive IJP in 2016.^[83] Although green solvents have poor solubility and produce lower efficiency compared to fabricated PSCs with organic solvents such as DMF, they are ecofriendly and are preferred for large-scale manufacturing. In their research, lead (II) acetate trihydrate [$\text{Pb}(\text{OAc})_2 \cdot 3\text{H}_2\text{O}$] and $\text{CH}_3\text{NH}_3\text{I}$ aqueous solutions were used as reactive inks to form the perovskite layer; in consequence, the PCE over 3.73% was achieved. Mathies et al fabricated and optimized PSCs by the multipass digital IJP approach.^[84]

The number of printed sublayers and the drop spacing were controlled with digital IJP, which influenced perovskite film thickness and crystal size. In addition, a vacuum annealing process was used for extracting excess solvents and forming uniform perovskite film. The multipass printing approach of the one-step MAPbI₃ ink for the formation of a perovskite layer is displayed in Figure 4j. Figure 4k presents AFM images of MAPbI₃ printed on FTO/ TiO_2 substrates after annealing at 100 °C.

The analysis included evaluating different printing parameters such as the number of depositing processes and dropping spacing. It was noticed that increasing these parameters led to a larger grain size. When printing multiple layers, the first layer dried and formed seed crystals, while the subsequent layer partially dissolved the surface and allowed crystals to grow from the seed crystals. Additionally, an image of the spin-cast layer was provided for comparison with the IJP perovskite films. The efficiency and reproducibility of PSCs with 11.3% were found to be higher with better crystallinity and homogeneity of the light harvester layer. In 2018, the same research group used a noncontact IJP technique to create PSCs with triple-cation perovskite layers containing 10% in a mixed composite.^[85] The thickness of the perovskite film was varied between 175 and 780 nm by modifying the drop distance during IJP. SEM cross-sectional images of IJP triple-cation PSCs with different absorber layer thicknesses in various drop spacing are shown in Figure 4l. The size of the grain and its thickness tend to increase when the drop spacing is decreased due to solvent annealing. The PCE of 12.9% with more stability and heat resistance was demonstrated for best inkjet-printed PSCs with a thickness of 520 nm in ambient conditions.

Generally, solvent evaporation in the nonscalable spin-coating method is faster than in printed techniques; in addition, the anti-solvent has been used for the formation of extremely uniform and dense perovskite layers.^[27,86] However, IJP method is applicable for large-area PSCs, where the rate of solvent evaporation is critical for perovskite crystallites. Furthermore, the vacuum-assisted process can accelerate the evaporating of solvents and produce a perfect and dense perovskite thin film. Liang et al. in 2018 achieved a pure-phase, high-quality MAPbI₃ perovskite layer using the one-step IJP method, along with the vacuum-assisted processing and thermal annealing post-treatment.^[87] After printing perovskite precursor solution, the liquid film was transformed into a vacuum heating chamber and exposed to a pressure of 50 Pa for a duration of 2 min. The purpose was to facilitate the rapid crystallization of the perovskite through a technique called vacuum flashing and thermal annealing. In addition, carrier extraction performance and surface wettability of the low-temperature TiO_2 substrate were optimized by treating it with buckminsterfullerene (C₆₀). The PCEs of inkjet-printed PSCs with 5 nm C₆₀ interlayer with percentages of 17 and 13.3 were obtained for active area sizes of 0.04 and 4 cm², respectively, with high stability and scalability.

In 2018, Li and co-workers covered mp- TiO_2 with a homogeneous PbI₂ film, resulting in a compact perovskite film with microscale crystalline grains.^[88] A uniform liquid membrane was created using precisely controlled microdroplets through IJP. Furthermore, limited random diffusion of the precursor solution enabled them to obtain a homogeneous PbI₂ film and in consequence a compact perovskite film. The uniform perovskite layer led to high PCEs of 18.64% for a small active area (0.04 cm²) and 17.74% for a large active area (2.02 cm²).

In addition to the two-step method for depositing perovskite, a one-step method was used in IJP technique. In 2019, Schlisske et al. demonstrated tuning the color perception and freedom in the design of the PSC's shape with the bright color of luminescent downshifting layers (LDS) by IJP.^[89] Color photovoltaics, with different shapes, variable translucency, and flexible designs,

will be fascinating to utilize in the building or automotive market. LDS layers work by absorbing high-energy photons from the solar spectrum, which has lower quantum efficiency than visible range.

Organic fluorescent dyes exhibit emission in the visible wavelengths that escape from the device and reach the human eye. The results demonstrated that application of luminescent materials of various colors can be achieved with a relatively small ($\approx 17\%$) reduction of PCE. In the same year, Eggers and co-workers demonstrated enabling of unprecedentedly high PCEs over 21% and stabilized power output efficiencies of about 18% for inkjet-printed PSCs.^[76] Generally, three key challenges were considered to ameliorate cell performance in IJP technique. First, the solvent composition was engineered to achieve optimal printability of perovskite film. Second, wetting of printed ink droplets and charge carrier extraction in charge transport layer were optimized. Third, nucleation and crystallization of perovskite wet film to form a highly crystalline perovskite layer, for example, by vacuum-assisted crystallization, are controlled.^[72,86]

SEM images of cross sections of inkjet-printed PSCs with different resolutions are shown in **Figure 5a**. It can be observed that the thick IJP perovskite thin films possess a columnar crystal structure, without any horizontal grain boundaries, which extends throughout the thickness. The thickness of the perovskite thin film varies from ≈ 400 nm (600 dpi) up to nearly 4 μm (2000 dpi).

In 2020, Li et al. were able to decrease the amount of perovskite defects through retarding the crystallization rate of the perovskite layer via ink engineering of IJP perovskite layer.^[90] The printing solvent consisted of n-methyl pyrrolidone (NMP) and DMF, and PbX_2 was replaced by $\text{PbX}_2\text{-DMSO}$ ($X = \text{Br}, \text{I}$) complex. Figure 5b shows a schematic diagram of inkjet-printed perovskite films, which shows four different strategies of ink engineering references processed on the substrate glass/ITO/ NiO_x . Top-view SEM images of the IJP perovskite film based on different ink systems are illustrated in **Figure 5c**. The new ink system created a high-quality perovskite layer with high homogeneity and large grain size (over 500 nm). Subsequently, the efficiency of PSCs by combining mentioned advantages were about 19.6% (0.04 cm^2) and 17.9% (1.01 cm^2). The devices with a lower defect concentration retained their original efficiency of 89% after being exposed to air for 1000 h. In 2021, PSCs with the all-inkjet-printed absorber and charge transport layers were recorded by Schackmar et al.^[91] A high-quality IJP triple-cation perovskite layer with columnar crystal structures was deposited with exceptional thicknesses of 1 μm . The inkjet-printed PSCs with p-i-n-architecture and nickel oxide hole transport layer demonstrated PCE of over 17%. The PSC exhibited a stable short-time-operated ($>40\text{ h}$) PCE at 85 °C with no loss in efficiency.

In 2022, Pathak and co-workers optimized $\text{Cs}_{0.05}\text{FA}_{0.79}\text{MA}_{0.16}\text{Pb}(\text{Br}_{0.17}\text{I}_{0.83})_3$ PSCs with inks containing the polymer PTB7 as an additive in both spin-coating and IJP deposition methods.^[92] The results exhibited that PSCs with the IJP technique have higher differences between samples with and without the polymer ink additive compared to the spin-coating method. The polymer PTB7 affected the crystallization dynamics of the perovskite layer in the IJP method and improved the quality of the resulting perovskite layers. In comparison, the PCE of

8.0% reached 10.35% for cells prepared with the polymer additive. Yang et al. controlled the perovskite film quality by solvent engineering technique in IJP method in 2022.^[93] Formamidinium iodide (FAI) is completely dissolved in a mixture of n-butanol and isopropanol (IPA) in order to react with films made of PbI_2/CsBr . When n-butanol is added to IPA solvent, drying time is prolonged and it prevents the contact line from getting pinned. Ultimately, the inkjet-printed $\text{Cs}_x\text{FA}_{1-x}\text{Pb}(\text{I},\text{Br}_{1-y})_3$ perovskite film with large grain size and high uniformity achieved a PCE of 18.26% in 0.15 cm^2 active area.

The comparison of the published IJP deposition techniques in PSCs is summarized in **Table 2**. Wide studies have been introduced about utilizing IJP technique in PSCs, which demonstrates that that is a promising method for scalable and highly efficient solar cells. The contactless and mask-free properties of this technique give us the ability to design our favorite patterns with lowest damage to the substrate. Moreover, the IJP technique consumes less material compared to spin-coating methods, and green solvents can be used in perovskite precursor.^[94] Cost-effectiveness and ecofriendliness are essential parameters for economical manufacturing procedures. However, IJP has certain limitations such as slow deposition speed and the possibility of nozzle clogging.^[95] Despite all the challenges, IJP is a bright technique for commercializing the new generation of perovskite photovoltaic devices.

4. Screen-Printing Technique

Screen-printing technique is another popular method for depositing various layers of nanostructured devices. In this coating technique, meshes have been equipped with different sizes of stencils defining the printing pattern. This method includes two types of flatbeds and rotary screen printing.^[96] In the flatbed screen-printing technique, a squeegee swipes over the screen to transfer the ink through the mesh. The repeating process is required to deposit a high-quality layer. In the rotary screen-printing technique, the resolution, printing speed, and achievable wet thickness are better than flatbed screen printing. However, in the first studies on perovskite photovoltaic devices, the perovskite absorber layer was coated on a mesoporous TiO_2 photoanode in a liquid electrolyte-based electrochemical cell.

A variety of device architectures has been introduced for solid-state PSCs, such as n-i-p structures and p-i-n structures. Typically, in n-i-p or normal structures, first metal oxides like TiO_2 , SnO_2 , and ZnO are deposited as ETLs on FTOs or ITOs.^[97] Then, perovskite absorber layer, scaffold layer, and HTL are coated on the substrate and finally, Au or Ag metal back contact is deposited on HTL. **Figure 6a** illustrates schematics of the screen-printing technique for coating ETL, scaffold layer, and carbon layer films for printable mesoscopic applications.

Figure 6b exhibits a schematic structure and the cross-sectional SEM image of the screen-printed scaffold.^[98] In the p-i-n architecture, which is known as an inverted structure, first p-type layer is coated on ITO or FTO. Then, perovskite film and after that n-type ETL are deposited on the substrate, respectively.

Metal back contact commonly used in PSCs presents low chemical stability and high costs, which are the main barriers to large-scale production of perovskite devices. Therefore, a

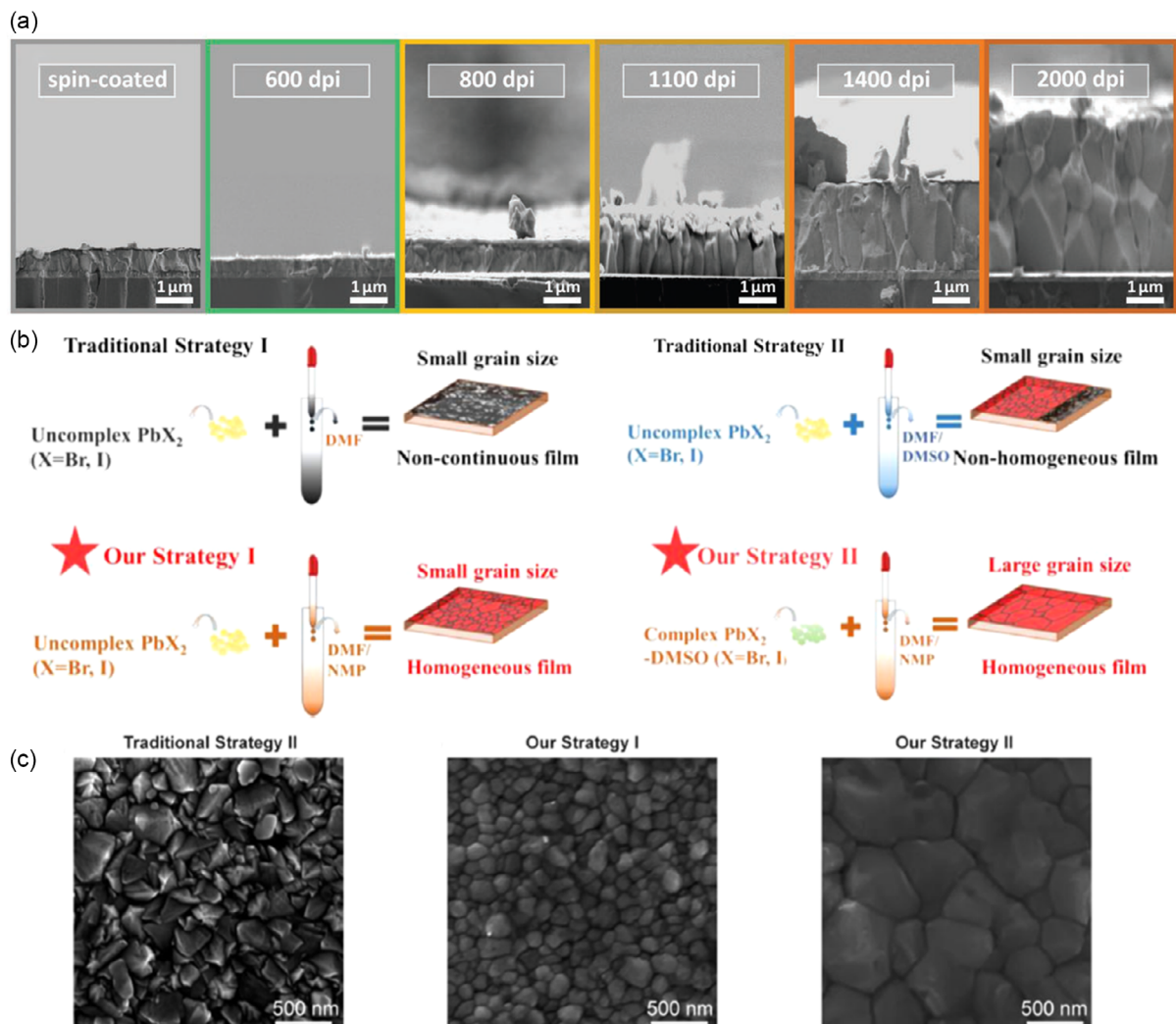


Figure 5. a) SEM images of cross sections of PSCs with IJP perovskite absorber layers printed at different resolutions. Spin-coated reference samples were also included. Reproduced with permission.^[77] Copyright 2019, Advanced Energy Materials, Wiley. b) Schematic diagram of perovskite films that have been printed using an inkjet printer. It describes four strategies of processing ink engineering references on the substrate of glass/ITO/NiO_x. Reproduced with permission.^[90] Copyright 2020, ACS Applied Materials Interfaces, ACS. c) Top-view SEM images of the inkjet-printed perovskite film using various ink systems Reproduced with permission.^[90] Copyright 2020, ACS Applied Materials Interfaces, ACS.

low-cost carbon-contact layer with proper work function is utilized on mesoporous-insulating layer using the screen-printing technique in the fabrication process. Followed by preparing the scaffold, the perovskite solution is dropped onto the carbon electrode and infiltrated into the scaffold.

In 2013, Ku et al. reported an efficiency of 6.64% using this structure and screen-printing technique for the first time in PSCs.^[99] Figure 6c displays the schematic of the crystal structure of CH₃NH₃PbI₃ perovskite, structure of a carbon-based monolithic device, and the corresponding energy levels of different layers. In 2014, a fully printable HTL-free mesoscopic solar cell was developed by Rong et al. The best PCE of up to 10.64% was obtained from this inexpensive photovoltaic device.^[100]

In another study, Liu and colleagues were able to boost efficiency by over 39% using NiO as the HTL in the TiO₂/NiO/

carbon structure in 2015.^[16] NiO enhanced the photocurrent and open-circuit voltage, leading to an efficiency of 11.4% under AM1.5G conditions. Chan and co-workers utilized solvent extraction crystal growth for highly efficient HTL-free carbon-based mesoscopic PSC.^[101] They developed a drop-casting method utilizing solvent extraction to achieve the growth of dense and uniform perovskite nanocrystals at room temperature. Perovskite solution (40% in NMP) was dropped onto the pre-heated (70 °C) mesoporous substrate with TiO₂/Al₂O₃/C layers. After 10 min at 70 °C, the substrate was immersed in diethyl ether at 25 °C for 30 min to complete the solvent extraction process. The solvent extraction precursor implemented homogeneous nucleation of perovskite inside the mesoporous layers. The PCE of 12.3% was achieved for printable HTL-free carbon-based mesoscopic PSCs and continued to exceed 12% for 5000 h in 2016.

Table 2. Literature overview of PSCs that applied the IJP deposition technique in the fabrication process and coating perovskite layer.

Structure	PCE [%]	V _{OC} [V]	Active area [cm ²]	Coating methods for different layers	Coating process of perovskite film	References
ITO/NiO _x /Cs _{0.1} MA _{0.15} FA _{0.75} Pb(I _{0.85} Br _{0.15}) ₃ /C ₆₀ /bathocuproine (BCP)/gold	21.6	1.11	1	Electron beam evaporation/IJP/evaporation/thermal evaporation	One step using different solvents GBL, DMF, and DMSO	[77]
FTO/TiO ₂ /CH ₃ NH ₃ PbI ₃ /Nanocarbon	11.6	0.95	Not mentioned	TiCl ₄ treatment/spin coating and dip coating/IJP	Two steps adding carbon to CH ₃ NH ₃ I ink	[79]
FTO/TiO ₂ /CH ₃ NH ₃ PbI ₃ /CH ₃ NH ₃ PbCl ₃ /spiro-OMeTAD/Au	12.3	0.91	0.04	Spin coating/IJP/spin coating/thermal evaporation	One step adding MACl in the printing solution	[80]
ITO/PEDOT:PSS/perovskite/PCBM/Al	11.1	0.87	Not mentioned	Spin coating /IJP/spin coating/thermal evaporation	Two steps mixing multiple cations via multichannel IJP	[81]
ITO/PEDOT:PSS/CH ₃ NH ₃ PbI ₃ /PCBM/Al	3.73	0.87	Not mentioned	Spin coating/reactive IJP /spin coating/thermal evaporation	One step using multichannel IJP for perovskite precursor	[83]
FTO/TiO ₂ /CH ₃ NH ₃ PbI ₃ /spiro-OMeTAD/Au	11.3	1	0.135	Spin coating/digital IJP/spin coating/thermal evaporation	One step using digital IJP	[83]
FTO/TiO ₂ /Cs _{0.1} (FA _{0.83} MA _{0.17}) _{0.9} Pb(Br _{0.17} I _{0.83}) ₃ /spiro-OMeTAD/Au	12.9	1.13	0.09	Spin coating/IJP /spin coating/Thermal evaporation	One step control perovskite morphology by variation of the drop spacing.	[85]
FTO/TiO ₂ /C ₆₀ /CH ₃ NH ₃ PbI ₃ /spiro-OMeTAD/Au	13.3	1.08	4	TiCl ₄ treatment/thermal evaporation/IJP/spin coating/thermal evaporation	One step using vacuum-assisted thermal annealing post-treatment and optimized solvent composition.	[87]
FTO/TiO ₂ /CH ₃ NH ₃ PbI ₃ /spiro-OMeTAD/Au	17.74	1.08	2.02	Spin coating/IJP/spin coating/thermal evaporation	Two steps controlling microdroplets by IJP	[88]
FTO/TiO ₂ /Cs _{0.1} (FA _{0.83} MA _{0.17}) _{0.9} Pb(Br _{0.17} I _{0.83}) ₃ /spiro-OMeTAD/Au	21	1.05	0.09	Spin coating/IJP /spin coating/thermal evaporation	One step	[89]
FTO/TiO ₂ /C ₆₀ /Perovskite/spiro-OMeTAD/Au	14.5	1.1	4.04	TiCl ₄ treatment/thermal evaporation/IJP/spin coating/thermal evaporation	One step using new mixed-cation perovskite ink system	[90]
ITO/NiO _x /Cs _{0.10} FA _{0.75} MA _{0.15} Pb(Br _{0.15} I _{0.85})/PCBM/BCP/Au	12.3	1.02	1	IJP/IJP/IJP/thermal evaporation	One step fully IJP PSCs	[91]
ITO/SnO ₂ /Perovskite+PTB7/spiro-OMeTAD/Au	10.35	1.07	Not-mentioned	Spin coating/IJP /spin coating/Thermal evaporation	One step using polymer additive	[92]
ITO/SnO ₂ /Perovskite/spiro-OMeTAD/Au	18.26	1	0.15	Spin coating/thermal evaporation and IJP /spin coating/thermal evaporation	Two steps using mixed ink composition	[93]

Photovoltage of triple-mesoscopic PSCs was increased with the post-treatment of mesoporous scaffolds by Sheng in 2020.^[102] Post-treatment of the triple-mesoscopic base on TiO₂/ZrO₂/carbon architecture caused a shift in the conduction band of the mp TiO₂ layer from -4.22 to -4.11 eV. This shift facilitated electron transfer from perovskite absorber layer to TiO₂ ETL, resulting in an improved V_{OC} of 1.02, FF of 0.7, and PCE of 16.51%. These PSCs demonstrated reasonable stability, 91.7% of the initial efficiency after 1000 h of continuous operation at the maximum power point under AM1.5G one sun illumination. The results suggest that employing the screen-printing technique simplifies the production of effective PSCs with mp charge transport layers, due to its simple procedure and significant photovoltage improvement. In 2021, Alon and co-workers observed the highest reported efficiency of 15% using two-step deposition of perovskite in all-printable mesoporous carbon-based PSCs.^[98] After dropping the PbI₂ + PbBr₂ solution, the dipping time of FAI + MABr solution was tuned to prepare a highly stable perovskite layer, and the best time was about

20 min. Figure 6d displays an EDS line scan of a solar cell's cross section, revealing the perovskite elements throughout the device structure. Iodine, bromine, and lead are detected from the top to bottom layers.

In 2022, Raptis and et al. fabricated highly scalable, stable, and low-cost fully printable carbon-based PSCs.^[103] The pinhole-free screen-printed compact layers, with optimum thickness were investigated and compared with TiO₂ compact layer deposited via spray pyrolysis. Accordingly, TiCl₄ treatment of compact layer was used to reduce surface traps and charge recombination at the TiO₂/perovskite interface in PSCs. Furthermore, TiCl₄ treatment improved the quality of the screen-printed films and increased PCE of 11.86 to 13.11% with the corresponding devices.

The screen-printing method due to low viscosity and instability of perovskite links presents challenges for coating the perovskite layer. Most published papers using the screen-printing method focus on printing ETL, HTL, and carbon electrodes. In 2022, Chen et al. concentrated on depositing the perovskite layer using the screen-printing technique.^[104] They employed

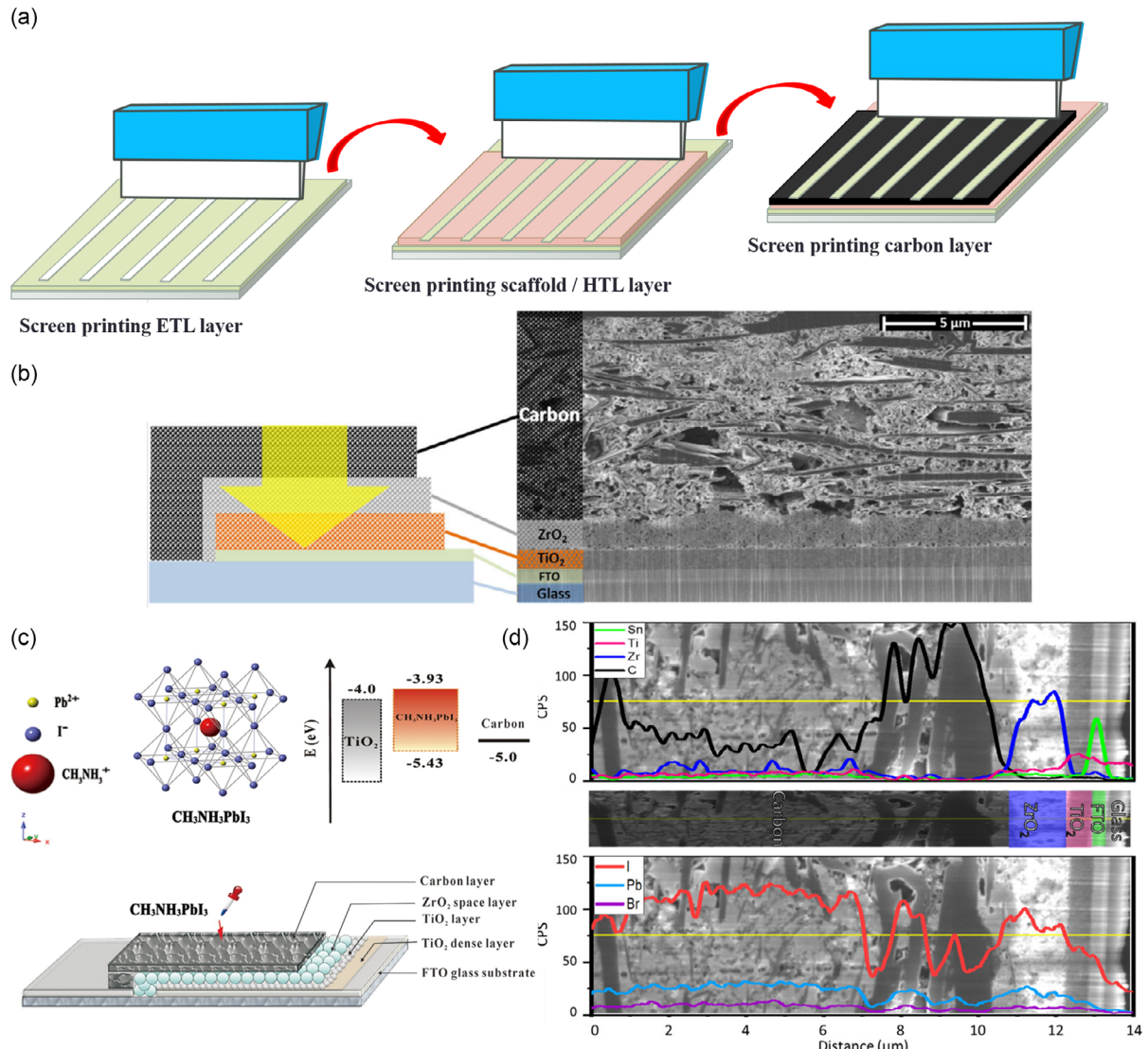


Figure 6. a) Schematic of screen-printing technique for coating ETL, scaffold layer, and carbon layer films toward printable mesoscopic. b) A schematic structure and cross-sectional SEM image of the screen-printed scaffold. Reproduced with permission.^[98] Copyright 2021, Solar RRL, Wiley. c) CH₃NH₃PbI₃ perovskite crystal structure and the corresponding energy levels of TiO₂, CH₃NH₃PbI₃, and carbon. Reproduced with permission.^[99] Copyright 2013, Scientific Reports, Nature. d) EDS line scans of cross section of the PSC. The various elements are indicated in different colors in the figure. Reproduced with permission.^[98] Copyright 2021, Solar RRL, Wiley.

methylammonium acetate ionic liquid solvent with higher viscosity to prepare the perovskite inks and address low-viscosity issues. The cohesive and adhesive ink improved the printing quality and efficiency, thereby enhancing the overall performance. This was enabled by a methylammonium acetate ionic liquid solvent which stabilized and adjusted the viscosity of the perovskite ink, with a viscosity range of 40–44 000 cP. The thickness of the perovskite thin film was controlled from about 120 nm to about 1200 nm, from 0.5 × 0.5 to 5 × 5 cm², and patterned on different substrates. The best efficiencies of 20.52% (0.05 cm²) and 18.12% (1 cm²) were obtained with the screen-printing technique in ambient air conditions. The obtained PCEs were comparable with efficiencies of 20.13% (0.05 cm²)

and 12.52% (1 cm²) for the spin-coated thin films in normal devices with thermally evaporated metal electrodes.^[104]

In 2022, Kamino and co-workers strived to remove evaporated metallization of the front contact instead of the industry standard screen-printed silver grids.^[105] They applied a low-temperature silver paste (\approx 140 °C) for the front-metal grid of two-terminal perovskite–silicon tandem structures by the screen-printing process. Finally, they achieved a steady-state efficiency of 22.6% over an aperture area of 57.4 cm².

In summary, we observed that screen printing method is another depositing technique of thin films based on the solution process, which can be used in ambient conditions. **Table 3** summarizes the published screen-printing coating techniques in

Table 3. Literature overview of utilization of the screen printing deposition technique in coating mesoscopic structure ETLs, HTLs, and contact electrodes in PSCs.

Structure	PCE [%]	V _{OC} [V]	Active area [cm ²]	Coating methods for different layers	Coating process of perovskite	References
FTO/TiO ₂ /ZrO ₂ /Perovskite/carbon	15	0.93	0.085	Spin coating and TiCl ₄ treatment/screen printing for other layers	Two steps modifying the perovskite precursors' concentration and the dipping time	[98]
FTO/TiO ₂ /ZrO ₂ /CH ₃ NH ₃ PbI ₃ /carbon	6.64	0.878	0.125	Spray pyrolysis/screen printing for other layers	One step using spheroidal graphite	[99]
FTO/TiO ₂ /ZrO ₂ /CH ₃ NH ₃ PbI ₃ /carbon	10.64	0.868	0.13	Spray pyrolysis/screen printing for other layers	Two steps using TiO ₂ nanosheets	[100]
FTO/TiO ₂ /Al ₂ O ₃ /CH ₃ NH ₃ PbI ₃ /carbon	12.3	0.846	0.09	Spray pyrolysis/screen printing for other layers	One step using solvent extraction crystal growth	[101]
FTO/TiO ₂ /ZrO ₂ /CH ₃ NH ₃ PbI ₃ /carbon	16.5	1.02	0.1	Spray pyrolysis/screen printing for other layers	Using post-treatment method with 2-Phenyl-5-benzimidazole sulfonate-Na	[102]
FTO/TiO ₂ /ZrO ₂ /CH ₃ NH ₃ PbI ₃ /carbon	12.87	0.9	0.49	Screen printing compact ETL and TiCl ₄ treatment/screen printing for other layers	One step using 5-ammonium valeric acid iodide	[103]

PSCs. Generally, screen printing technique has been used for mesoporous structures, and it is a proper method for pastes or highly viscous ink. The thickness and structure of mesoporous layers have an important impact on pore filling and device performance. Full screen-printed layers with high-quality, pin-hole-free surfaces and lower surface traps could facilitate the industrialization of PSCs. Coating of the photoactive absorber layer by scalable printing technologies demonstrates the great potential of perovskite technology for industrial applications. However, cleaning the meshes after coating may impose a higher cost on the application of screen-printing technology. Moreover, transferring the ink through the mesh requires swiping squeegee over the screen and repeating the process. Therefore, flatbed screen printing is more time-consuming than rotary screen printing for large-scale roll-to-roll processing.

5. Slot-Die-Coating Technique

One of the most suitable routes for deposition of large-area thin films with uniform and homogenous coverage is slot-die coating.^[106] In this process, the substrate moves across the slot die head, which is very close to the substrate. The schematic of slot die-coating process is represented in Figure 7a, where ink is pumped into the die using a syringe pump and distributed toward the slot. While the ink is forced out the narrow slot, it fills the gap between the head and moving substrate, finally forming a wet layer of ink on the substrate. After evaporation of the solvent, a uniform thin film is formed on the substrate. The waste of materials in this method is lower than other methods such as spin coating and spray pyrolysis. Moreover, the wet film's thickness can be accurately controlled by adjusting the ink flow rate of ink into the die and the speed of the moving substrate.^[107–109]

The perovskite absorber layer is the most important layer in the PSCs. Therefore, good crystallinity with a large grain size of the perovskite film results in uniform coverage with the fewest defects and imperfections. Like other coating techniques in the

slot die-coating method, two procedures including one or single-step and two-step or sequential deposition process have been used for coating perovskite thin films. The two-step deposition process is identical in both slot die coating and spin-coating methods.

First, the PbI₂ precursor is slot die coated on the substrate and then dried followed by MAI solution deposition onto the PbI₂ layer by slot die coating or dip coating.^[110–113] On the other side, in one step deposition, perovskite layer is deposited from a single precursor.^[114–116] Schmidt et al. studied how these two methods affect the slot die-coated perovskite film on the flexible substrate.^[117] They found that the sequential method is more sensitive to the substrate change in comparison with the one-step method while scaling up in p-i-n structure, where the PCE changed from 9.4% to 4.9% with the upscaling process. However, the sequential method is more affected by altering the deposition from spin coating to slot die roll-to-roll coating.^[118,119] Generally, TCOs have been utilized for PSCs while they have high rigidity, weight, and fragility, which make a barrier for roll-to-roll processing on a large scale.^[120] Additionally, the film drying mechanism in slot die coating is dissimilar to spin coating.^[121] In spin coating, the extra solution spreads simultaneously when the substrate spins and the wet film dries while spinning continues at high speed. However, in slot die coating, the solution can flow and lose uniformity during drying and then a highly nonuniform film forms due to slow drying.

In order to accelerate the solvent evaporation, a nitrogen (N₂) gas jet is employed to externally speed up the film's drying.^[122] In 2015 for the first time, Hwang et al. fabricated a fully slot die-coated PSC using gas quenching.^[123] In this technique, a flow of compressed nitrogen gas on the just-deposited wet film causes accelerated solvent drying with the second slot head added to the first slot.

Finally, dense PbI₂ is formed on the substrate through gas quenching. The naturally dried PbI₂ film has a less uniform appearance, while the gas-quenched PbI₂ film has a glassy appearance. The difference between the gas-quenched PbI₂ film

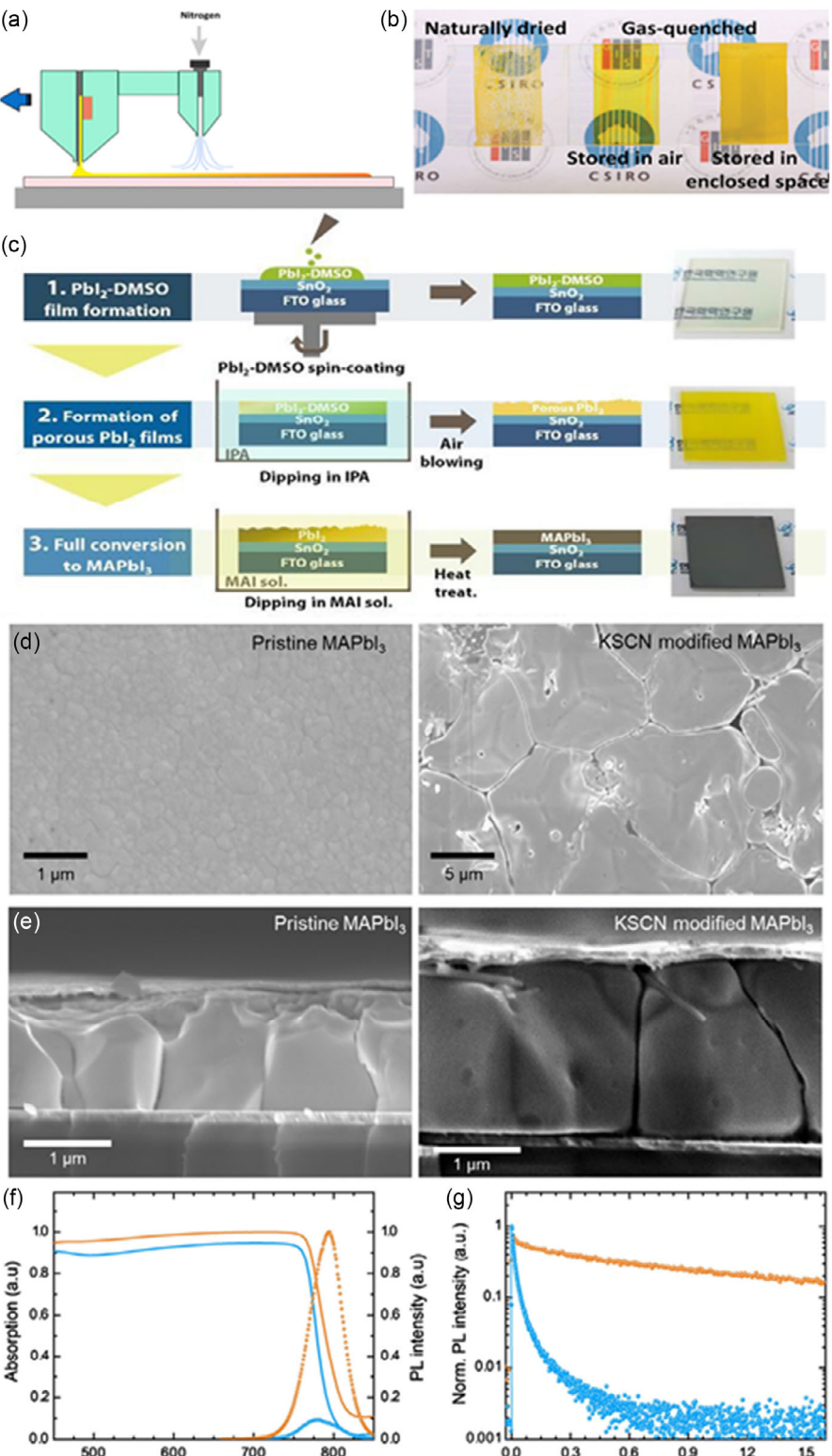


Figure 7. a) Schematic of the slot die-coating technique. b) The effect of different gas-quenching strategies on PbI_2 film. Reproduced with permission.^[124] 2015, Advanced Materials, Wiley. c) Schematic diagram of the MET procedure and optical images of the resulting films. Reproduced with permission.^[139] 2018, Journal of Materials Chemistry A, RSC. d) Top-view and e) cross-sectional SEM of pristine and KSCN-modified MAPbI_3 films deposited on PTAA. Reproduced with permission.^[143] 2021, Small Science, wiley. f) Absorptance, steady-state PL, and g) TRPL spectra of pristine and KSCN-modified MAPbI_3 films.^[143] 2021, Small Science, wiley.

and PbI_2 film dried under ambient conditions is shown in Figure 7b. Furthermore, to achieve a dense and compact perovskite layer, efficient diffusion of MAI through the PbI_2 film is necessary. A dense PbI_2 film imposes weak penetration of MAI; consequently, the PbI_2 film poorly converts to the perovskite film. To solve this problem, the dense PbI_2 film was soaked in the vapor solvent in an enclosed chamber. This method causes the formation of more porosity within PbI_2 film, resulting in converting to perovskite film efficiently. The cloudy PbI_2 film has microcracks that allow MAI to permeate through PbI_2 film and forms a dense perovskite layer. The whole slot-die PSCs reached the efficiency of 11.96%; moreover, the main disadvantage of this technique is that the storage is time-consuming, which is not appropriate to scale up the process.

DMF, N-methylpyrrolidone (NMP), DMSO, and GBL are the typical solvents for the perovskite ink.^[124–127] DMF and DMSO are usually used for the preparation of the perovskite precursor; however, due to their toxic nature, these solvents are unsuitable for mass production. These solvents facilitate the growth of perovskite crystals by the formation of the intermediate phase.^[128,129] DMSO is less toxic than DMF; however, due to its high surface energy and high boiling point, its wettability on the most substrates is lower than that of DMF. Generally, perovskite film quality such as crystallinity, uniformity, and surface morphology has direct influence on cell performance. Hence, many strategies have been developed to regulate the one-step deposition of perovskite films. These include hot casting, antisolvent quenching, gas quenching, and processing additives.^[86,130–137]

In 2017, Jung and et al. optimized cell performance by improving solidification dynamics of the perovskite precursor solutions into the crystallized films.^[138] Due to the rapid evaporation of DMF and different solubilities between MAI and PbI_2 which result in MAI– PbI_2 –DMF formation, the needle-like morphology of perovskite film is formed. Thus, by adding N-cyclohexyl-2-pyrrolidone (CHP) to DMSO in precursor solvent, crystallization occurs at an optimum speed. CHP with a high boiling point and low vapor pressure produced a homogenous perovskite layer with better performance and PCE of 12.56%. Galagon and co-workers demonstrated the feasibility of upscaling PSCs technologies to high volume production using roll-to-roll slot die coating. Besides, the addition of 10% vol 2-butoxyethanol reduces the surface tension of DMSO solution; subsequently, it improves the wettability and coverage of the perovskite precursor on the substrate.^[127] Ultimately, the best value obtained for the manufacturing of flexible PSCs with roll-to-roll deposition technology was over 13.5%.

Kim et al. in 2018 first reported mediator extraction treatment (MET) for PbI_2 deposition to reach the high-quality perovskite layer in sequential deposition method.^[139] The complete conversion of compact PbI_2 layer to perovskite layer required a long reaction time in the two-step coating technique. Additionally, the compact and high-crystalline PbI_2 layer prevented in converting the whole inner parts of lattice to perovskite film. Therefore, changing the morphology of the compact PbI_2 film to a macroscopically porous scaffold allowed for rapid and effective penetration of the MAI solution, resulting in complete conversion to a perovskite film over a large area. Figure 7c schematically shows the entire procedure of the MET and heat treatment process for

fabricating the perovskite film. In this method, dissolved PbI_2 in DMF:DMSO (9:1) is slot die coated on the substrate, then compressed air flow is used to form $\text{PbI}_2 + \text{DMSO}$ complex. DMSO mediator is extracted by dipping in IPA bath; afterward, the wet film is converted to a perovskite film by dipping in MAI solution. The MET process, dipped in IPA, created a relatively randomized crystal orientation compared to heat treatment with specific orientation. The randomized crystal orientation of PbI_2 produced a porous structure which accelerated the penetration of MAI solution into the PbI_2 layer. Finally, the maximum PCE of 18.3% was obtained in $10 \times 10 \text{ cm}^2$ FTO for porous PbI_2 with slot die coating.

Another challenging layer in upscaled PSCs is HTL. The most used p-type material as organic HTLs in n-i-p architecture is 2,2',7,7'-Tetrakis(N,N-di-p-methoxyphenylamine)-9,9'-spirobifluorene (spiro-OMeTAD). It shows highest performance for hole extraction in PSCs; despite that, it is expensive and hydrophilic due to using lithiumbis (trifluoromethanesulfonyl) imide.^[140,141]

Due to the slow drying process in the slot die technique, the weak wettability of spiro-OMeTAD is more critical compared with spin coating. Researchers have presented solutions in order to overcome the limitation of spiro-OMeTAD. One of these solutions abovementioned is the fabrication of HTM-free carbon-based PSCs in which the mesoporous carbon layer is used as scaffold.^[142] In this structure, the perovskite precursor infiltrates through the micrometer-thick mesoporous scaffold due to capillary force. The infiltration of perovskite precursor occurs from carbon to ETL, and then perovskite phase simultaneously nucleates and grows in the pores. In slot die coating of perovskite, infiltration through the mesoporous scaffold and evaporation compete with each other. In high-speed movement of the die, the precursor infiltration may lag behind the precursor casting, resulting in pores being left free from the precursor. On the other hand, if the die moves so slowly, the bead will crystalize at the front of the slot and prevent the further infiltration of precursor. In this situation, evaporation occurs faster than infiltration. At moderate moving speeds, the precursor continuously infiltrates into the pores of the scaffold, leading to concurrent infiltration and evaporation.

Xu et al. fabricated slot-died triple-mesoscopic PSCs with different speed movements of dies (slow: $< 5 \text{ mm s}^{-1}$; moderate: $10\text{--}15 \text{ mm s}^{-1}$; fast: $> 20 \text{ mm s}^{-1}$).^[125] A maximum PCE of 12.87% on an active area of 60.08 cm^2 was obtained at intermediate moving speed; with short-circuit current density of 22.49 mA cm^{-2} .

F. Xu and co-workers improved the crystal size and quality of slot die-coated perovskite film via additive engineering using potassium thiocyanate (KSCN).^[143] Figure 7d,e shows top-view and cross-sectional SEM images of pristine and KSCN-modified MAPbI₃ films deposited on PTAA. Potassium can effectively passivate surface defects. KSCN was applied as an additive in MAPbI₃ precursor solutions. KSCN enlarged crystal grain sizes significantly up to $11 \mu\text{m}$; eliminated defects in perovskite film; and increased charge carrier parameters that are comparable with single-crystal perovskites. To examine optical characterizations such as absorptance, steady-state PL, and TRPL spectra, refer to Figure 7f,g. The films modified with KSCN demonstrate notably higher PL intensity compared to the pristine MAPbI₃.

films, indicating the elimination or passivation of defects that act as nonradiative recombination centers. Reducing crystal defects improves all carrier-related parameters by eliminating both recombination and scattering centers for charge carriers. The TRPL spectra showed an increase in carrier lifetime from 0.16 μ s to a maximum of 1.89 μ s. Maximum PCE of 21.38% was achieved for planar inverted PSCs with negligible hysteresis. Recently, Abate et al. were able to create reproducible and uniform perovskite films at room temperature without controlling humidity, using a slot die coater.^[144] They employed a novel artificial peptide, sulfonyl- γ -AApeptide (F-GLU-S), to modify the perovskite surface, grain boundaries, and electronic defects. F-GLU-S has multifunctional components including carbonyl, carboxyl, sulfonyl, benzene, and chloro groups, which effectively interacted with the perovskite layer and repaired the uncoordinated Pb²⁺ ions and halide vacancies. As a result, the slot die-coated perovskite device demonstrated outstanding performance, achieving efficiency of 21.44% with remarkable moisture stability.

Giacomo and co-workers demonstrated scalable sheet-to-sheet slot die-coating processes for PSCs and modules in 2018.^[145] The drying condition and annealing atmosphere were crucial for the perovskite layer processed using the slot die method to exhibit the same morphology as the one produced through one-step spin coating. The process was modified to produce large-area modules (168.75 cm²) with efficiencies exceeding 10%. In order to deposit a high-quality perovskite layer in a large area, Liu's group applied high-pressure nitrogen-extraction strategy.^[146] The formation of an intermediate solid film or perovskite film during solvent evaporation depends on thermal annealing and drying conditions.^[147] High-pressure nitrogen-extraction method had a significant impact on solvent evaporation and formation of fully crystallized perovskite thin film. The film that was solidified without any post-treatments was mostly amorphous. However, the perovskite layer that underwent high-pressure nitrogen extraction exhibited significant crystallinity and was primarily composed of the yellow nonperovskite phase. Eventually, they extended controlled printing to assemble perovskite solar modules with an area of 40 \times 40 mm², and the best PCE was 19.6% for an active area of 7.92 cm².

In 2022, Xu et al. reported by slot die coating an efficient triple-halide perovskite absorber with optimized bandgaps of 1.63 eV.^[95] Excellent optoelectronic properties and no-phase segregation were obtained with adding 5 mol % of MAPbCl₃ into the double-cation perovskites Cs_{0.22}FA_{0.78}Pb(I_{0.85}Br_{0.15}). Thus, perovskite single-junction cells that are coated with slot-die techniques have achieved high stability and performance. These cells were able to reach a stabilized power output of 19.4%. Additionally, they integrated the halide perovskites into tandem architecture with industrial silicon bottom cells, which demonstrated scalable industrially relevant perovskite silicon tandem solar cells with PCE of 25.2% on a 1 cm² active area. Li et al. recently conducted a study to eliminate the ribbing effect in slot die coating and adjust the viscosity of precursor ink.^[148] They achieved this by adding acetonitrile, a low-viscosity cosolvent, to n 2-methoxyethanol-based FAPbI₃ precursor inks. The team was able to achieve a PCE of 17.1% for an active area of 12.7 cm². Additionally, the encapsulated devices exhibited great stability, nearing 100% for 1 year.

A comparison of published slot die coating techniques in PSCs and modules is tabulated in Table 4.^[86,95,111–151] In summary, the slot die coating method with its optimization is an efficient and high-throughput technique for creating compact perovskite layers. This method is compatible for roll-to-roll production of large-area perovskite photovoltaics. However, controlling the uniformity and crystallization quality of thin films is challenging over a large area. In general, thermal annealing and drying conditions have a significant impact on perovskite layer. Moreover, the addition amount of solvent dramatically changes perovskite thin-film morphology and crystallinity. The stream of nitrogen has been applied in drying wet perovskite films to avoid the use of antisolvents and produce high reproducibility as well. Upscaling PSCs will be reproducibly manufactured with high performance by optimizing parameters such as speed of movement and solvents.

6. Spray Coating

Spray coating is another solution-based deposition technique for large-area photovoltaic devices. In this method, precursor solution spreads across a substrate via shear forces.^[152] Therefore, it is significantly faster and cheaper than other manufacturing process. In comparison with the lab-scale deposition method via spin-coating technique, the spray-coating technique widely attracts exploration on scalable PSCs. Already spray coating is extensively utilized in the industry which is its remarkable advantage for high volume, as well. Despite the benefits of spray coating, there are several challenges like ink perpetration with low concentration, optimization of fluid flow rate, the height or speed of the spray head, and the temperature of the substrate being coated.^[153] In the deposition process, the droplets wet the surface, and then the substrate is heated to evaporate the solvent from the layer. The surface tension of ink is an important factor for the contact angle of droplet and substrate and the consequence on thin-film quality. In addition, ink density, droplet size, velocity, viscosity, and nature of the substrate affect formation of the uniform layer.^[154,155]

Spray-coating techniques like other deposition methods use the “one-step” or “two-step” deposition process for the organic-inorganic perovskite layer. In a series of published papers on the two-step spray-assisted perovskite coating process, typically, the spin-coating technique was used for deposition of inorganic PbI₂ in the first stage.^[156–160] Then, organic solution was sprayed onto the surface to form perovskite thin film. In contrast to the high efficiencies of these types of PSCs, the wasteful spin-coating technique is limited to the scalability process.

To fabricate large-area PSCs based on solution processing, Huang and co-workers developed a two-step ultrasonic spray deposition.^[161] In ultrasonic spray, piezoelectric transducers at the nozzle tip generate high-frequency vibrations. These high-frequency vibrations create capillary waves in a liquid film that increase the uniformity of droplet size and film formation. The application of ultrasonic spray in their work produced a uniform and smooth centimeter-scale of perovskite CH₃NH₃PbI₃ film. Figure 8 demonstrates a schematic diagram of the two-step spray method for the deposition of perovskite CH₃NH₃PbI₃ film. First, the dissolved PbI₂ in DMSO was ultrasonically sprayed onto the

Table 4. Comparison of published PSCs and modules that utilized slot-die technique in fabrication process and coating perovskite layer.

Structure	PCE [%]	V _{OC} [V]	Active area [cm ²]	Coating methods for different layers	Coating process of perovskite	References
FTO/ETL/Cs _{0.05} MA _{0.4} FA _{0.55} Pb(I _{0.96} Br _{0.04}) ₃ /Spiro-OMeTAD/Au	15.9	1		Spray pyrolysis/spin coating/slot-die coating/spin coating/thermal evaporation	Two steps optimizing the deposition parameters	[111]
ETL ₁ : SnO ₂	18.4	1.06	12			
ETL ₂ : compact-TiO ₂ /SnO ₂	16.7	1.07				
ETL ₃ : compact-TiO ₂ /meso-TiO ₂						
ITO/SnO ₂ /Cs _{0.1} (MA _{0.15} FA _{0.85}) _{0.9} Pb(I _{0.85} Br _{0.15}) ₃ /spiro-OMeTAD/Ag	10.57	0.98	0.07	Roll-to-roll microgravure printing/slot die coating/spin coating/thermal evaporation	Two steps roll-to-roll printing technology enables flexible PSCs under ambient conditions	[112]
ITO/SnO ₂ /Cs _{0.1} (MA _{0.15} FA _{0.85}) _{0.9} Pb(I _{0.85} Br _{0.15}) ₃ /Spiro-OMeTAD/Ag	13	1	1	Full roll-to-roll printing of PSC Full slot die coating	Two steps improving crystallinity and morphology by nitrogen blowing and controlling substrate temperature	[113]
	15.1	1.03				
FTO/c-TiO ₂ /m-TiO ₂ /MAPbI _{3-x} Cl _x /Spiro-OMeTAD/Au	9.2	0.73	0.0625	Spray pyrolysis/bar coating/slot die coating/spin coating/thermal evaporation	One step postprocessed rapid air knife application to appropriate crystallization of perovskite film	[114]
ITO/poly-TPD/MAPbI ₃ /PCBM/Au	3.3	0.96	0.16	Full roll-to-roll printing of PSCs	One step using a polymer starch template to assist the perovskite growth	[116]
ITO/PEDOT-PSS/MAPbI _{3-x} Cl _x /PCBM/ZnO/Ag	4.9	0.9	0.2–0.5	Full roll-to-roll printing of PSCs	One step printing back electrode	[117]
ITO/ZnO/PCBM/MAPbI ₃ /P ₃ HT/PEDOT:PSS/Ag	2.6	0.81				
ITO/PEDOT-PSS/C3-SAM/MAPbI _{3-x} Cl _x /PCBM/ZnO/Ag	5.1	0.98	0.5	Full slot die coating	One step applying 3-aminopropanoic acid to modify the crystallinity and coverage of perovskite film	[118]
ITO/ZnO/MAPbI ₃ /BifluOMeTAD/MoO ₃ /Ag	14.7	1.1	0.1	Full slot die coating	Two steps using amorphous Biflu-OMeTA as HTL	[119]
ITO/ZnO/MAPbI ₃ /spiro-OMeTAD/MoO ₃ /Ag	11.7	1.06				
ITO/PEDOT:PSS/MAPbI _{3-x} Cl _x /PCBM/Ag	2.91	0.68	0.12	Full slot die coating	One step fabrication of flexible PSCs in ambient condition and low temperature	[120]
FTO/NiO _x /MAPbI ₃ /PCBM/TBAOH-SnO ₂ /Au	14.3	1.01	1.44	Full slot-die coating	One step dynamic thermal annealing using once-thorough process	[121]
FTO/SnO ₂ /FA _{0.84} Cs _{0.16} PbI _{2.83} Br _{0.17} /Spiro-OMeTAD/Au	18	1.02	0.09	Spin coating/slot die/spin coating/thermal evaporation	One step using Methylammonium-free precursor	[122]
ITO/ZnO/MAPbI ₃ /P3HT/Ag	11.96	0.95	0.1	Full slot-die coating	Two steps using N gas blowing to rapidly evaporate the solvent	[123]
ITO/PEDOT-PSS/Cs _{0.1} (MA _{0.15} FA _{0.85}) _{0.9} Pb(I _{0.85} Br _{0.15}) ₃ /PCBM/LiF/Ag	13.41	0.97	0.12	Full roll-to-roll slot-die coating	One step using antisolvent processing	[126]
ITO/SnO ₂ /Cs _{0.15} FA _{0.85} PbI _{2-x} Br _x /spiro-OMeTAD/Au	15.2	1.029	0.09	Full roll-to-roll slot die coating	One step performance by nontoxic solvents at ambient temperature	[127]
ITO/PEDOT:PSS/MAPbI _{3-x} Cl _x /PCBM/BCP/Ag	12.2	0.75	7.84	Full roll-to-roll slot-die coating	One step using acetonitrile/methylamine solvent	[128]
FTO/NiMgLiO/FA _{0.83} Cs _{0.17} PbI _{2.83} Br _{0.17} /LiF/C ₆₀ /BCP/Bi/Ag	16.63	1.084	20.77	Spray coating/slot die/thermal evaporation	One step enhance the nucleation barrier by diphenyl sulfoxide(DPSO)	[129]
FTO/TiO ₂ /Cs _{0.17} FA _{0.83} Pb(I _{0.83} Br _{0.17}) ₃ /Spiro-OMeTAD/Au	17.5	1.14	0.09	Spin coating/slot die/spin coating/thermal evaporation	One step introduction of methylammonium chloride in the precorsore formulation	[137]

Table 4. Continued.

Structure	PCE [%]	V _{OC} [V]	Active area [cm ²]	Coating methods for different layers	Coating process of perovskite	References
ITO/PEDOT-PSS/MAPbI ₃ /PCBM/BCP/Ag	12.52	1	0.10	Spin coating/slot die/spin coating/thermal evaporation	One step addition of cyclohexyl-2-pyrrolidone (CHP) and dimethyl sulfoxide (DMSO) to perovskite ink	[138]
ITO/FrGO/MAPbI ₃ /PCBM/BCP/Ag	9.57	0.87				
FTO/SnO ₂ /MAPbI ₃ /spiro-OMeTAD/Au	18.8	1.12	0.096	Spin coating/slot die/spin coating/thermal evaporation	Two step producing porous PbI ₂ by MET	[139]
FTO/c-TiO ₂ /m-TiO ₂ /m-ZrO ₂ /carbon/Cs _{0.05} (FA _{0.4} MA _{0.6}) _{0.95} PbI _{0.8} Br _{0.2}	17.02	1.08	0.129	Full slot die coating	One step cosintering of layers for increased manufacturing speed	[142]
ITO/PTAA/KSCN -MAPbI ₃ /C ₆₀ /BCP/Ag	21.38	1.11	0.089	Blade coating/slot die coating/thermal evaporation	One step improved using potassium thiocyanate as additive	[143]
FTO/TiO ₂ /MAPbI _{3-x} Cl _x /spiro-OMeTAD/Au	16.8	1.03	0.09	Full sheet-to-sheet slot die coating	One step laser ablation processes for conventional monolithic cell interconnections	[145]
FTO/TiO ₂ /FA _{0.91} Cs _{0.09} PbI ₃ /M4N[BF ₄]/PCBM/Ag	22.7	1.12	7.92	Chemical bath deposition/slot die coating/thermal evaporation	One step using high-pressure nitrogen extraction to assist crystallization	[146]
ITO/2PACz (SAM)/MAPbI ₃ /C ₆₀ /BCP/Cu	20.55	1.13	2.2	Spin coating/slot die coating/thermal evaporation	One step using 2-methoxy-ethanol and dimethyl-sulfoxide based ink	[147]
FTO/SnO ₂ /Cs _{0.16} FA _{0.84} Pb(I _{0.88} Br _{0.12}) _{35%} +5% mol MAPbCl ₃ /spiro-OMeTAD/Au	18	1.02	0.09	Spin coating/slot die coating/thermal evaporation	One step varying annealing conditions to improve single junction and tandems	[95]
ITO/MeO-2PACz/FAPbI ₃ /LiF/C60/SnO _x /Cu	22.54 17.1	1.088 5.36	1.58 12.7	spin coating/slot die/thermal evaporation/thermal evaporation	One step to study rheological properties of the precursor inks	[148]
ITO/NiO _x /MAPbI ₃ /PCBM/BCP/Cu	11.68	1.98	2.1	All slot die coating	One step in an inverted structure	[149]
ITO/NiO _x /Cs _{0.2} FA _{0.8} PbI ₃ /PCBM/BCP/Cu	14.9	2.03				
FTO/SnO ₂ /3-cation perovskite/spiro-OMeTAD/Au	13.5	0.939	0.09	Spin coating/hybrid slot die-evaporation/spin coating/thermal evaporation	Two steps using hybrid slot die coating and thermal evaporation technique	[150]
FTO/NiO _x /MAPbI ₃ /PCBM/PEI	13.86 13.54	Not mentioned	0.09 0.75	All slot die coating	One step using nontoxic solvent at room temperature	[151]

FTO/TiO₂ substrate at 60 °C. In the second step, the solution of CH₃NH₃I in isopropanol is sprayed onto the PbI₂ film at 80 °C. In the final step, to promote the reaction and crystallization of CH₃NH₃PbI₃, the as-prepared film was heat treated. Large-area perovskite layer with higher smoothness showed better crystallinity and thermal stability, resulting in efficiency of 13.09% for the large area of 1 cm².

Jiang et al. fabricated perovskite solar minimodules in using the two-step deposition technique with a combination of raster ultrasonic spray coating and chemical vapor deposition (CVD).^[162] In the first stage, lead iodide layer was deposited by the raster-scanned ultrasonic spray coating method with negligible Pb-waste compared to the spin-coating method. To create a FAPbI_xBr_{3-x} perovskite, the organic components composed of formamidinium bromide (FABr), FAI, and MACl are incorporated via CVD in the next stage. Ultimately, the environmental-friendly and transferable technique to the industry produced a high-quality and uniform perovskite and PCE of 14.7% for 12 cm² modules.

In utilizing a one-step spray-coating technique, Barrows et al. explored the initial work for depositing a CH₃NH₃PbI_{3-x}Cl_x perovskite solution in inverted architecture PSCs in 2014.^[163]

This group deposited the perovskite absorber layer in a single-spray pass using an ultrasonic system onto a heated substrate under ambient conditions. After annealing in air and crystallization of the perovskite film, best efficiency of 11% was achieved. The sensitive role of the substrate temperature was investigated on perovskite morphology and on the efficiency of the resultant solar cells during spray casting, as well. In 2015, Das et al. produced a highly uniform and efficient surface coverage of the perovskite layer with an high-throughput ultrasonic spray-coating process.^[164] The highly crystalline and uniform CH₃NH₃PbI_{3-x}Cl_x films produced PCE of 13% on the glass substrate. In addition, the deposition process at low temperatures was investigated on the polyethylene terephthalate (PET) substrates PCE as high as 8.1% was exhibited. The reasonable cell performance on the PET substrate demonstrated that spray-coating technique is an efficient method for flexible PSCs.

In 2016, Tait and co-workers demonstrated that ultrasonic spray coating was a scalable and versatile linear deposition technique for high-efficiency perovskite photovoltaic.^[165] The combinations of Pb-containing precursors (Pb(CH₃COO)₂·3H₂O, PbI₂, and lead chloride (PbCl₂)) with CH₃NH₃I were sprayed to deposit MAPbI₃ perovskite absorber layer. Ratios and concentrations of

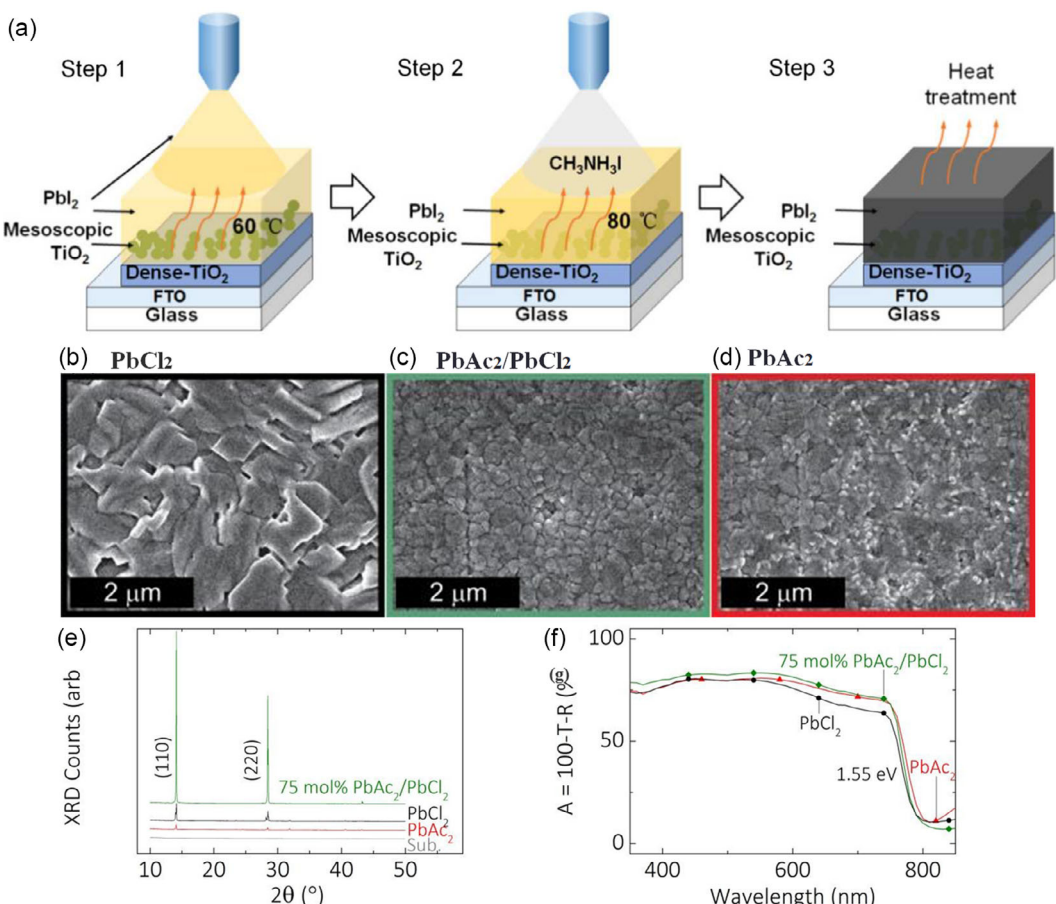


Figure 8. Schematic diagram of the two-step spray method for coating perovskite $\text{CH}_3\text{NH}_3\text{PbI}_3$ film. Reproduced with permission.^[153] 2017, Scintific Reports, nature. SEM images of perovskite films sprayed from inks of b) PbCl_2/MAI , c) concurrently pumped PbAc_2/MAI with PbCl_2/MAI at 75 mol% PbAc_2 , and d) PbAc_2/MAI . e) XRD (equally scaled with arbitrary units) and f) absorbance ($A = 100 - T - R \%$) spectra for each layer with an optical bandgap of 1.55 eV. The reference substrate is also included in the XRD. Reproduced with permission.^[165] 2016, Journal of Materials Chemistry A, RSC.

perovskite precursors are essential factors for controlling the crystallinity and overall morphology. SEM images, XRD, and absorbance spectra (where $A = 100 - T - R \%$) were utilized to examine the characteristics of sprayed perovskite films, as shown in Figure 8b–d. The mixed precursors displayed greater consistency in the crystal lattice compared to single precursors. Ultimately, highly crystalline and pinhole-free layers produced initial PCE of 15.7% for small-scale devices and 11.7% for 3.8 cm² modules. In the same year, Heo et al. utilized a new approach to fabricate spray-coated PSCs, in which they sprayed the solution of MAPbI_3 in DMF and GBL solvents onto a substrate held at 120 °C continuously.^[166] The continuously sprayed perovskite solution moistened the underlying polycrystalline perovskite layer. The small perovskite grains were partially redissolved and merged in the solvent blend and then regrown, and reaching micrometer-length scales. The novel perovskite-coating technique produced the efficiency of 15.5% for 40 cm² modules.

Similar to other coating techniques, perovskite film quality greatly depends on nucleation during solvent evaporation. Heat treatment and various solvent evaporation rates play a critical role in nucleation and as a result, in the formation of a

compact and uniform perovskite layer. In 2018, Lidzay's group fabricated triple-cation-based PSCs with a peak PCE of 17.8% using a combination of ultrasonic spray coating and vacuum-assisted solution processing.^[167] Utilizing low vacuum removed trapped solvent and initiated crystallization through controlled nucleation; the produced perovskite films had comparable quality with those produced via spin coating. In 2019, Cai's group applied both an antisolvent extraction method and addition of MnCl_2 additives to perovskite ink.^[168] They were able to achieve horizontal grain boundary-free perovskite films by the spray-coating method. Ultimately, the PCE of 15.07% was obtained for square-centimeter rigid device PSCs and 13.21% for flexible PSCs. Comprehensively understanding of the nucleation, crystallization, and growth process was attempted in another work of Cai group.^[169] The thickness of the perovskite thin film was systematically optimized by the antisolvent bath and thermal annealing time. Nonpolar diethyl ether was used as an antisolvent to extract polar precursor solvents in the wet film. Higher nucleation density and improved coverage were promoted in the low-temperature processes for perovskite films. After optimization of spray conditions, a high efficiency of 20.6% was attained

under ambient conditions. The PCE of 19.4% was obtained on a small area with fully spray-cast PSCs in another work of Lidzay's group in 2020.^[170] An ultrasonic spray coater operated inside a nitrogen-filled glovebox and low-humidity air, which showed control drying and crystallisation dynamics of the perovskite layer. Perovskite thickness was optimized via fluid flow rate, head height, and velocity across the substrate. The PCE of 12.7% was achieved by connecting seven 15.4 mm² devices in parallel on a single substrate in active area of 1.08 cm².

In Table 5, the comparison of published spray-coating technique in PSCs is arranged. The spray-coating method has advantages compared to other scalable techniques; it is a faster technique and spray head can move across a substrate at more than 5 m per minute.^[152] Optimizing complex parameters such as solution flow rate, solvent choice, surface temperature, and spray head height and speed is essential for creating high-quality films. Moreover, ink preparation with higher concentration and viscosity is required to deposit the desired thickness of the perovskite.^[171] Spray-cast method suffers less from poor process reproducibility, scalability, and nearly time used in the fabrication of PSCs.

7. Physical Vapor Deposition Coating

Among the diversity of deposition mechanisms, physical vapor deposition (PVD) is another option for scaling up photovoltaic devices. The PVD process takes place in high vacuum, and then materials in vapor phase transfer to the substrate; after

condensation of vapor, a dense and uniform layer is produced. Evaporation and sputtering are the most known PVD methods for producing thin and dense films. Liu and his co-workers created simple planar heterojunction solar cells by integrating dual-source vapor deposition, which produced uniform flat films of the mixed-halide perovskite $\text{CH}_3\text{NH}_3\text{PbI}_{3-x}\text{Cl}_x$.^[172] The PCE of 15.4% demonstrated that perovskite absorbers can achieve high efficiencies in simple device designs without requiring complex nanostructures. Figure 9a shows a schematic illustration of the PVD setup with one, dual, and triple sources which include both organic and inorganic sources for coating the perovskite absorber layers. High-quality contacts and cost-effectiveness are important factors for large-scale solar cell manufacturing. Unfortunately, PVD technology is prepared under high vacuum conditions and high temperature; consequently, it uses lots of energy, time, and cost in production process. In 2017, Tong et al deposited a high-quality compact perovskite film via well-controlled lower temperature (<120 °C) and lower-temperature fast chemical vapor deposition (LFCVD) process within 20 min.^[173] Figure 9b shows the configuration of the low-temperature-zone furnace tube and the fabrication procedure of LFCVD for synthesizing perovskite film. Fan's group applied single-source thermal evaporation for coating $\text{CH}_3\text{NH}_3\text{PbI}_3$ perovskite thin film. The obtained large-area perovskite layers with 100 cm² area were nearly dense, uniform, and smooth. Although, due to the high volatility of organic cations at 150 °C, the optoelectronic properties and morphology were poor in large-area perovskites. Consequently, low PCEs of about 7.73% were achieved for these photovoltaic cells. The

Table 5. Comparison of published PSCs that applied spray-coating technique in the fabrication process and coating perovskite layer.

Structure	PCE [%]	V _{OC} [V]	Active area [cm ²]	Coating methods for different layers	Coating process of perovskite	References
FTO/TiO ₂ /CH ₃ NH ₃ PbI ₃ /spiro-OMeTAD/Au	13.09	1	1.0	Spin coating/ spray coating /spin coating/thermal evaporation	Two-step ultrasonic spray method	[153]
FTO/TiO ₂ /FAPbI _x Br _{3-x} /spiro-OMeTAD/Au	14.7	6	12.0	Sputtering/ spray coating and chemical vapor deposition/spin coating/thermal evaporation	Two-step combining raster ultrasonic spray coating and chemical vapor deposition	[154]
PEDOT:PSS/CH ₃ NH ₃ PbI _{3-x} Cl _x /PCBM/Ca/Al	11.1	0.92	0.025	Spin cast/ spray coating /spin coating/thermal evaporation	Optimization of processing parameter space	[155]
FTO/TiO ₂ /CH ₃ NH ₃ PbI _{3-x} Cl _x /spiro-OMeTAD/Ag	13	1.03	0.23	Spin coating/ spray coating /spin coating/thermal evaporation	One step ITO coated on PET substrates	[156]
ITO/TiO ₂ /CH ₃ NH ₃ (I _x Br _{1-x}) ₃ spiro-OMeTAD/Au	11.7	3.31	3.8	Electron beam evaporation/ spray coating /spin coating/thermal evaporation	One step using combinations of Pb-containing precursors	[157]
FTO/TiO ₂ /CH ₃ NH ₃ PbI _{3-x} Cl _x /PTAA/Au	15.5	10.5	40.0	Spray coating / spray coating /spin coating/thermal evaporation	One step using controlled composition of the solvents	[158]
ITO/np-SnO ₂ /perovskite/spiro-OMeTAD/Au	15.4	1	0.16	Spray coating / spray coating /Spin coating/thermal evaporation	One step using vacuum treatment	[159]
ITO/SnO ₂ /perovskite/spiro-OMeTAD/Au	15.07	1.138	1	Spin coating/ spray coating /spin coating/thermal evaporation	One-step antisolvent extraction and addition of MACl additives to perovskite ink	[160]
ITO/SnO ₂ /perovskite/spiro-OMeTAD/Au	20.6	1.2	1.0	Spin coating/ spray coating /spin coating/thermal evaporation	Optimization of coating parameters	[161]
ITO/nanoparticle SnO ₂ /triple-cation perovskite/spiro-OMeTAD/gold.	12.7	1.06	1.08	Spray coating /thermal evaporation	One step full spray coating	[162]

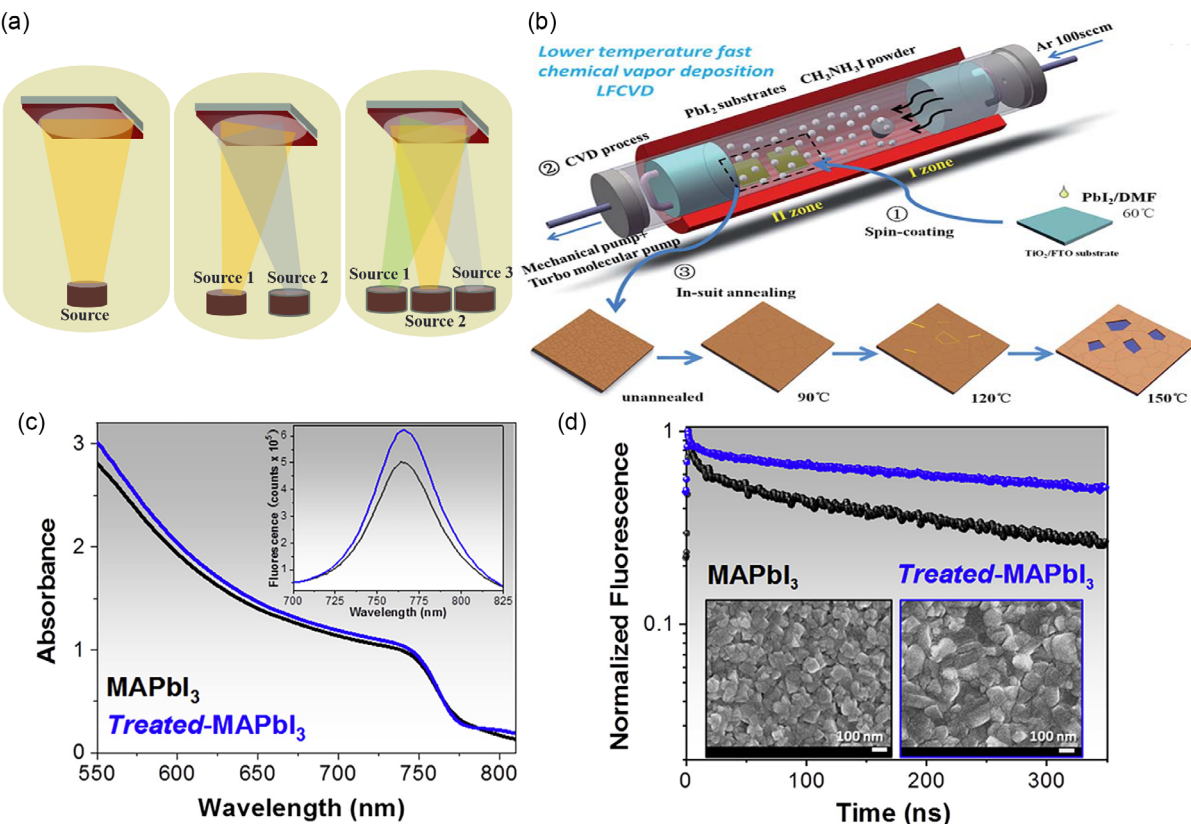


Figure 9. a) One-, dual-, and triple-source thermal evaporation systems which include both organic and inorganic sources for coating the perovskite absorber layers. b) Schematic diagram of the synthesizing procedure of perovskite ($\text{CH}_3\text{NH}_3\text{PbI}_3$) films with the configuration of the low-temperature-zone furnace tube and the LFCVD process. Reproduced with permission.^[173] Copyright 2017, RSC Advances, Royal Society of Chemistry. Thermally evaporated pristine MAPbI₃ (black line) and treated MAPbI₃ (blue line) thin-film characterizations: c) Absorption and PL spectra (in the inset) and d) TRPL decays. Top-view SEM images are reported in the inset. Reproduced with permission.^[174] Copyright 2020, Joule, Cell Press

PSCs obtained an efficiency of 15.1% in 120 °C and exhibited excellent air-exposure stability for more than 60 days without requiring specific encapsulation. Li and et al. fabricated the excellent scalability of thermal coevaporated PSCs. They combined strategies such as active layer engineering, surface treatments, interfacial optimization, and light management.^[174] Figure 9c,d shows the absorbance, PL spectra, TRPL measurements, and top-view SEM images of the coevaporated materials. The absorption and PL spectra of MAPbI₃ exhibit a distinct absorption peak at a bandgap of 1.61 eV and a PL peak at 780 nm, both before and after the treatment procedure. The defect passivation and reduction in nonradiative recombination led to an increase in PL intensity and fluorescence lifetime observed in the TRPL measurements. Ultimately, the PCEs as high as 20.28% and 19.0% were achieved for 0.1 and 1 cm² PSCs and a PCE value of 18.13% for a 21 cm² minimodule was recorded. FAPbI₃ shows higher thermal stability than MAPbI₃, despite its weaker phase stability. At temperatures below 150 °C, FAPbI₃ underwent a transition from the cubic black α -phase to a hexagonal yellow δ -phase. A research group led by Xie aimed to create pure and stable α -FAPbI₃ that underwent a rapid and complete phase transition from the δ -phase to the α -phase.^[175] To achieve this, they introduced high humidity (relative humidity [RH]: 75% \approx 90%) during the sequential

vapor deposition of the perovskite thin film. The energy difference between the two phases decreased under humidity, which accelerated the transformation to a pure δ -phase instead of a mixture of α - and δ -phases. After annealing the pure δ -phase perovskite thin film, a pure α -phase of FAPbI₃ was formed. The enhanced purity of the δ -phase and moisture led to the swift phase transition to pure α -phase during subsequent annealing. High-quality, vapor-deposited pure α -FAPbI₃ PSCs achieved a PCE of over 20%. The process of moisture-induced phase transition demonstrated excellent repeatability and increased the size of the thin film.

Wang et al. described a two-step coating method to produce uniform and dense CsFA-based perovskite films without MA.^[176] Initially, they spin coated a blend of lead halide and cesium halide and then thermally evaporated FAI under vacuum. Their research revealed a maximum PCE of 24.1% under standard AM1.5G illumination for CsFA-based PSCs without MA. They also achieved a PCE of 22.8% for an aperture area of 1 cm² with great stability over 20 000 h of storage. In another study, Yi's group utilized a Cl alloy-mediated sequential vacuum deposition method to fabricate PSCs.^[177] Initially, cesium iodide (CsI), PbI₂, and PbCl₂ were simultaneously evaporated onto the substrate. In the subsequent stage, formamidinium iodide was deposited using a thermal evaporating process. They

documented efficiencies of 24.42% and 23.44% for devices with areas of 0.1 and 1 cm², respectively. The resulting perovskite films exhibited excellent coverage and morphology, leading to high-performance solar cells. The researchers attributed the improved efficiency to the use of the Cl alloy-mediated sequential vacuum deposition method, which allowed for precise control over the film formation and composition. After being stored in dry air for over 4000 h, the unencapsulated devices showed desirable stability with minimal reduction in performance. This study demonstrated the potential for further advancements in PSC technology through innovative fabrication techniques.

Some published vapor deposition techniques in PSCs are compared and summarized in **Table 6**. The table includes information on the deposition method, substrate, perovskite material, and device performance. It is a useful resource for researchers looking to optimize their PSC fabrication process. Generally, vapor deposition has a low environmental impact processing method by reducing the waste of perovskite precursor solutions and eliminating the use of harmful organic solvents. As mentioned earlier, solvent extraction from the wet perovskite layer poses a challenge in the printing technique. The main advantage of the PVD method is that the evaporation process does not require any incorporation of solvents, producing uniform and high-quality perovskite thin films directly from powders. The thickness of layers is controllable and repeatable. In other words, being solvent free makes this technique ecofriendly and less toxic, eliminating the utilization of toxic solvents such as DMF, CB, DMSO, and so on. These positive properties still make this technique a good option for scalable PSCs.

Additionally, in the PVD process, the patterns of designed solar cell pixels are flexible and easily accessible with the help of relative masks. The PVD method offers better control over the crystallization process, resulting in improved film morphology and reduced defect density. This ultimately leads to higher efficiency and stability of PSCs. While PVD is a controllable and repeatable thin-film coating method, the processing speed is too slow, which is inadequate for mass production costs. Nevertheless, due to its potential for large-scale production

and environmental benefits, the PVD method remains a promising approach for the fabrication of efficient and sustainable solar energy devices”.

8. Challenges and Outlook

The perovskite stability and coating process are essential challenges for industrious fabrication of hybrid perovskite photovoltaic. Some challenges in PSC technology include stability, toxicity, integration with existing infrastructure, and scaling up production. Although these cells can be produced using simple and low-cost methods, scaling up production to industrial levels remains a challenge. A variety of techniques have been used to prepare large-area PSCs and are aimed to emit the huge gap between lab and factory. As perovskite stability and the performance of the devices are approximately correlated with its quality and uniformity; deposition techniques have critical effects on scalable PSCs. The coating methods used for PSCs should be optimized to reduce time and material requirements, employ a straightforward and cost-effective technique, and yield uniform layers that fully cover the substrates. The common deposition technique in research laboratories is the spin-coating technique, which is irreproducible, wasteful, and produces nonuniformity for large-area PSCs. Therefore, alternative scalable deposition techniques were investigated for large-area production of hybrid organic-inorganic PSCs in this review paper. Blade-coating technique, IJP method, screen-printing technique, slot die-coating technique, spray-coating, and PVD methods are developing techniques for large-scale PSCs.

In the blade-coating technique, a blade moves over the surface and spreads the solution on the substrate; it is an economical method for large-area and perovskite solar modules. However, the adjustable and low cost of blade coating is convenient for small scale; there are some challenges for application of this method in large scale. Incomplete coverage, pinholes, and non-uniformity of perovskite layers lead to main issues utilizing blade coating. In addition, blade coating suffers from the automation process and ink supply. IJP technique commonly is used in the graphics and publishing industries, which environmentally is

Table 6. Comparison of published PSCs that deposited perovskite layer through vapor deposition technique.

Structure	PCE [%]	V _{oc} [V]	Active area [cm ²]	Coating methods for different layers	References
FTO/TiO ₂ /CH ₃ NH ₃ PbI _{3-x} Cl _x /spiro-OMeTAD/Ag	15.4	1.07	0.076	Spin coating/vapor deposition/spin coating/thermal evaporation	[172]
FTO/TiO ₂ /CH ₃ NH ₃ PbI ₃ /spiro-OMeTAD/Ag	15.1	1.03	0.1	Spin coating/vapor deposition/spin coating/thermal evaporation	[173]
FTO/SnO ₂ /PCBM/MAPbI ₃ /spiro-OMeTAD/Au	18.13	6.71	21	Spin coating/Spin coating/vapor deposition/spin coating/thermal evaporation	[174]
ITO/SnO ₂ /FAPbI ₃ /spiro-OMeTAD/Au	18.91	1.07	1	Spin coating/vapor deposition/spin coating/thermal evaporation	[175]
	20.19		0.1		
ITO/SnO ₂ /perovskit/spiro-OMeTAD/MoO ₃ /Au	22.8	1.16	1	Spin coating/Spin coating/vapor deposition/spin coating/thermal evaporation/thermal evaporation	[176]
	24.1		0.1		
FTO/SnO ₂ /perovskit/spiro-OMeTAD/Au	19.87	1.14	14.4	Spin coating/vapor deposition/spin coating/thermal evaporation	[177]
	24.42		0.1		

an effective fabricating method in printed electronics. IJP is demonstrated as a well-performed and noncontact strategy to prepare high-quality films. Optimization and configuration of devices and printing parameters are improved to enhance device performance. The IJP PSCs with acceptable efficiency and using lower material are promising for cheap and effective photovoltaic devices compared with spin-coated PSCs. Furthermore, IJP technique could be applied in tandem PSCs for more stable and highly efficient devices. Additionally, different materials could be incorporated into the perovskite solution to enhance grain boundaries and enhance resistance to light and humidity in the absorber layer, ultimately leading to the production of PSCs with satisfactory stability and efficiency. Solution engineering is an approach to improve the grain boundaries and crystallinity of perovskite film. The humidity and illumination stability of the absorber layer are directly affected by the crystallinity of the perovskite film. In another printing technique, screen printing has been used for depositing different layers of solar cells. Commonly, screen printing techniques have been utilized for carbon-based PSCs in ambient conditions. However, this is a cheap solution-processing method; the creation of compact and pinhole-free layers is a critical factor for depositing large-area perovskite photovoltaics. Solvent extraction from the precursor is an effective solution to improve the homogeneity nucleation of perovskite crystallites inside the mesoporous layers and prevent defect formation in perovskite film. Low-cost and versatile printing technologies demonstrate the promising potential of perovskite technology toward industrial applications. In slot-die coating method, ink is spread from a thin channel (metal die) over a moving surface. This coating process for solvent evaporation with low boiling point is suitable for plastic and flexible substrates, in particular in roll-to-roll deposition method. However, the formation of nonuniform films has been observed in this method due to the solution flowing and slow drying of solvents.

Therefore, a nitrogen gas jet is employed to accelerate the solvent evaporation and speed up the films drying.

The other simple and accessible technique for manufacturing PSCs is spray coating. Spray-coating method generally has been used in industrial paint equipment, wherein the precursor solution spreads over the substrate. Solution density, temperature, and ultrasonic atomization have an effect on nucleation and formation perovskite absorber layer. Besides the solution-based coating methods for perovskite films, the PVD technique with the vapor phase of the precursor materials is applied for scalable PSCs. This alternative technique due to high vacuum conditions is widely energy consuming. Although it produces pinhole-free and uniform layers, it is unsuitable and inefficient for commercializing perovskite photovoltaics.

In addition to the many challenges of depositing perovskite layers, depositing an HTL and an ETL is also a significant hurdle in producing scalable PSCs. While printing methods are effective and convenient for coating large areas of ETLs, they may pose difficulties in depositing organic HTLs. The spraycoating method is commonly used for coating the blocking layer in most articles. Developing a reliable and efficient method for depositing both the HTL and the ETL is essential for the commercialization of PSCs. However, achieving high quality in the perovskite layer is crucial for high efficiency and stability in devices, and therefore, the main concentration is on it. The current review focused on finding innovative solutions to overcome these challenges and improve the overall performance of the devices. Additionally, advancements in deposition techniques and material design were explored to enhance the scalability and stability of PSCs.

Figure 10 showcases the PCEs of up-scale PSCs and modules with an active area larger than 1 cm^2 . The inset graph provides a summary of the efficiency of PSCs and modules with different active areas. Despite these challenges, the outlook for PSCs is promising. Researchers are working on developing more stable

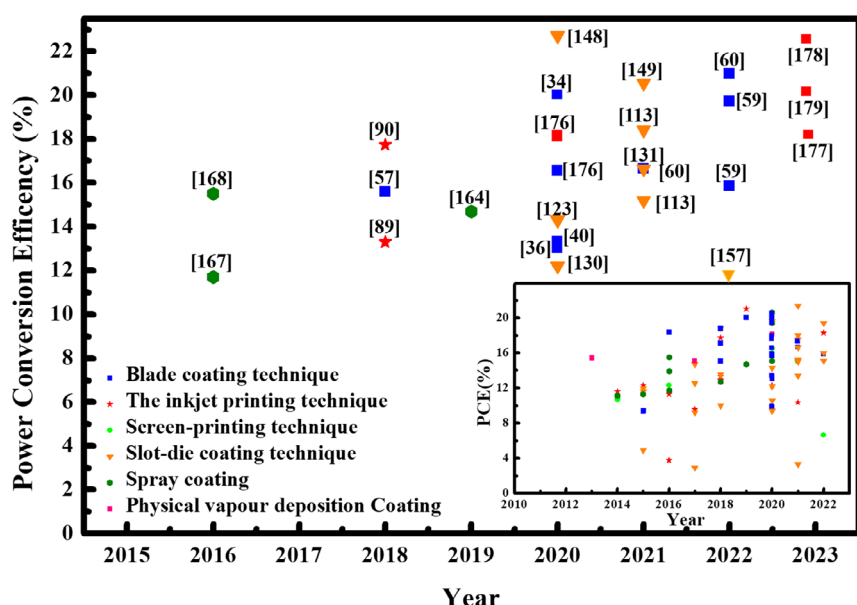


Figure 10. The PCEs of upscale PSCs and modules with active area larger than 1 cm^2 . The graph inset provides a summary of the efficiencies of PSCs and modules with varying active areas.

Table 7. The summary of advantages and challenges of various deposition techniques for coating of perovskite thin films.

Deposition technique	Advantages	Challenges
Blade-coating technique	Minimizing material usage, Adjustable and cost effective, Scalable technique	Limited by the automation process and ink supply Flow of the solution and losing uniformity
The inkjet-printing technique	Contactless and maskless, Appropriate for printing on uneven, curved, or pressure-sensitive surfaces, Low cost and low material consumption, Scalable technique	Limited by the slow coating speed and potential nozzle clogging, Producing destabilized and inhomogeneous layer
Screen-printing technique	Cost-effective, scalability, rapid film formation, Easy pattern, Reproducibility	Limited by inside cleaning and mesoporous layer architectures, Challenging with low viscosity of perovskite precursor solution
Slot-die coating technique	Scalable and compatible for roll-to-roll production in ambient condition, Avoid the using antisolvents, rapid and controllable with little solution waste	Limited by the time-consuming speed and ink supply, flow of solution and losing uniformity The risk of partial delamination of the perovskite film from the substrate
Spray coating	Fast and cheap method, controllable over film thickness and composition at relatively low temperatures	Limited by the waste materials, Ink perpetration and meticulous optimization
PVD coating	Dense and uniform layer reducing the waste of materials, Eliminating harmful organic solvents, Controllable and repeatable, High deposition rates, Capable to deposit various materials	Limited by the slow coating and time-consuming, Complex and high cost of maintaining high-vacuum environments, Limited by compatibility for temperature-sensitive substrates, Difficulties to control the deposition rate of organic halide materials at high vapor pressures

and efficient materials, as well as improving the manufacturing process. PSCs also have the potential to be used in a wide range of applications, including building-integrated photovoltaics and portable electronic devices.

9. Conclusion

In summary, various deposition techniques are investigated in scalable perovskite photovoltaics. High-quality and defect-free perovskite films cause a longer diffusion length for electrons and holes and consequently, higher filling factor with lower recombination.^[34–36] The comparisons of fabricated different PSCs via various techniques have indicated that solution-based methods are promising techniques for commercial hybrid organic–inorganic PSCs. The mixture of coating techniques, for instance, spray coating, slot-die coating, IJP, and screen printing, can be utilized for various layers and scalable perovskite photovoltaic devices. For instance, spray-coating method is proper for deposition of the blocking compact layer compared with the other technique. Printing deposition techniques are more controllable, economic, and appropriate for coating perovskite layer and other layers. On the other hand, the optimization process of perovskite coating with arbitrary compounds is more convenient in solution base processes than the physical coating method. However, perovskite solutions have a tendency to flow unevenly over the substrate due to their low viscosity, which can hinder achieving the desired thickness. This issue is common in most printing methods, thus necessitating drying and solvent extractions to ensure the production of high-quality perovskite films. Moreover, we have actively sought innovative approaches to address this challenge. **Table 7** provides a summary of the benefits and difficulties associated with different deposition techniques for coating perovskite films.

In addition to scalability techniques, the application of ecofriendly materials and solvents is a major challenge for scalable PSC technology. Using green solvents with nontoxicity and lead-free precursors shows promise as an alternative, particularly in printing slot-die coating, IJP, and screen-printing techniques.

Acknowledgements

M.A.-J. acknowledges the Department for Energy Security and Net Zero (project ID: NEXTCCUS), University College London's Research, Innovation and Global Engagement, and UCL Cities Partnerships Programme Award in Paris for their financial support. The authors acknowledge the ACT programme (Accelerating CCS Technologies, Horizon2020 project no. 691712) for financial support of the NEXTCCUS project (project ID: 327327). M.A.-J. and H.L. acknowledge Cornell-UCL Global Strategic Collaboration Awards team, UCL-IIT Delhi, and UCL- Indian Institute of Science for their financial Support. H.L. is grateful for support from the Chinese Scholarship Council (CSC) and the Faculty of Mathematical & Physical Sciences (MAPS) at University College London (UCL).

Conflict of Interest

The authors declare no conflict of interest.

Author Contributions

A.K. took care of conceptualization, methodology, validation, writing the original draft, and visualization. F.M. took care of conceptualization and writing the original draft. M.M. took care of review and Editing and supervision. H.L. took care of review and Editing. M.A.-J. took care of conceptualization, review and editing, and supervision.

Keywords

blade coating, inkjet printing, perovskite solar cells and modules, physical vapor depositions, screen printing, slot die coating, spray coating

Received: November 28, 2023

Revised: February 7, 2024

Published online:

- [1] A. S. R. Bati, Y. L. Zhong, P. L. Burn, M. K. Nazeeruddin, P. E. Shaw, M. Batmunkh, *Commun. Mater.* **2023**, *4*, 2.
- [2] A. S. R. Bati, A. A. Sutanto, M. Hao, M. Batmunkh, Y. Yamauchi, L. Wang, Y. Wang, M. K. Nazeeruddin, J. G. Shapter, *Cell Rep. Phys. Sci.* **2021**, *2*, 100598.
- [3] Y. Zhang, A. Kirs, F. Ambroz, C. T. Lin, A. S. R. Bati, I. P. Parkin, J. G. Shapter, M. Batmunkh, Thomas J. Macdonald, *Small Methods* **2021**, *5*, 2000744.
- [4] M. Abdi-Jalebi, Z. Andaji-Garmaroudi, S. Cacovich, C. Stavrakas, B. Philippe, J. M. Richter, M. Alsari, E. P. Booker, E. M. Hutter, A. J. Pearson, S. Lilliu, T. J. Savenije, H. Rensmo, G. Divitini, C. Ducati, R. H. Friend, S. D. Stranks, *Nature* **2018**, *555*, 497.
- [5] W. Zhou, T. Pan, Z. Ning, *Sci. China Mater.* **2022**, *65*, 3190.
- [6] Q. Lin, D. J. Kubicki, M. Omrani, F. Alamc, M. Abdi-Jalebi, *J. Mater. Chem. C* **2023**, *11*, 2449.
- [7] Y. Zhu, M. Hu, M. Xu, B. Zhang, F. Huang, Y. B. Cheng, J. Lu, *Mater. Futures* **2022**, *1*, 042102.
- [8] J. Feng, X. Zhu, Z. Yang, X. Zhang, J. Niu, Z. Wang, S. Zuo, S. Priya, S. (Frank) Liu, D. Yang, *Adv. Mater.* **2018**, *30*, 1801418.
- [9] Q. Hou, J. Ren, H. Chen, P. Yang, Q. Shao, M. Zhao, X. Zhao, H. He, N. Wang, Q. Luo, Z. Guo, *ChemElectroChem* **2018**, *5*, 726.
- [10] J. Park, J. Kim, H. S. Yun, M. J. Paik, E. Noh, H. J. Mun, M. G. Kim, T. J. Shin, S. I. Seok, *Nature* **2023**, *616*, 724.
- [11] E. J. Juarez-Perez, M. Wußler, F. Fabregat-Santiago, K. Lakus-Wollny, E. Mankel, T. Mayer, W. Jaegermann, I. Mora-Sero, *J. Phys. Chem. Lett.* **2014**, *5*, 680.
- [12] Z. Hu, Zh. Lin, J. Su, J. Zhang, J. Chang, Y. Hao, *Sol. RRL* **2019**, *3*, 1900304.
- [13] A. Khorasani, M. Marandi, A. Iraji zad, N. Taghavinia, *J. Alloys Compd.* **2023**, *936*, 168055.
- [14] A. Khorasani, M. Marandi, A. Iraji zad, N. Taghavinia, *Electrochim. Acta* **2019**, *297*, 1071.
- [15] A. Khorasani, M. Marandi, R. Khosroshahi, M. Malekshahi Byranvand, M. Dehghani, A. Iraji zad, F. Tajabadi, N. Taghavinia, *ACS Appl. Mater. Interfaces* **2019**, *11*, 30838.
- [16] Z. Liu, M. Zhang, X. Xu, L. Bu, W. Zhang, W. Li, Z. Zhao, M. Wang, Y. B. Chengac, H. He, *Dalton Trans.* **2015**, *44*, 3967.
- [17] T. Ji, Y. Wang, L. Feng, G. H. Li, W. Wang, Z. Li, Y. Hao, Y. Cui, *Rare Met.* **2021**, *40*, 2690.
- [18] Y. H. Zhang, Y. Li, *Rare Met.* **2021**, *40*, 2993.
- [19] J. Burschka, N. Pellet, S. J. Moon, R. Humphry-Baker, P. Gao, M. K. Nazeeruddin, M. Grätzel, *Nature* **2013**, *499*, 316.
- [20] Z. S. Almutawah, S. C. Watthage, Z. Song, R. H. Ahangharnejhad, K. K. Subedi, N. Shrestha, A. B. Phillips, Y. Yan, R. J. Ellingson, M. J. Heben, *MRS Adv.* **2018**, *3*, 3237.
- [21] N. J. Jeon, J. H. Noh, Y. C. Kim, W. S. Yang, S. Ryu, S. I. Seok, *Mater. Natl. Mater.* **2014**, *13*, 897.
- [22] J. Wu, X. Xu, Y. Zhao, J. Shi, Y. Xu, Y. Luo, D. Li, H. Wu, Q. Meng, *ACS Appl. Mater. Interfaces* **2017**, *9*, 26937.
- [23] J. Y. Shao, D. Li, J. Shi, C. Ma, Y. Wang, X. Liu, X. Jiang, M. Hao, L. Zhang, C. Liu, Y. Jiang, Z. Wang, Y. W. Zhong, S. F. Liu, Y. Mai, Y. Liu, Y. Zhao, Z. Ning, L. Wang, B. Xu, L. Meng, Z. Bian, Z. Ge, X. Zhan, Q. Meng, *Sci. China Chem.* **2023**, *66*, 10.
- [24] R. Swartwout, M. T. Hoerantner, V. Bulović, *Energy Environ. Mater.* **2019**, *2*, 119.
- [25] A. Khorasani, M. Marandi, A. Iraji zad, N. Taghavinia, *J. Mater. Sci.: Mater. Electron.* **2019**, *30*, 11576.
- [26] S. L. Hamukwaya, H. Hao, Z. Zhao, J. Dong, T. Zhong, J. Xing, L. Hao, M. M. Mashigaidz, *Coatings* **2022**, *12*, 252.
- [27] B. Parida, A. Singh, A. K. K. Soopy, S. Sangaraju, M. Sundaray, S. Mishra, S. F. Liu, A. Najar, *Adv. Sci.* **2022**, *9*, 2200308.
- [28] Z. Jiang, B. Wang, W. Zhang, Z. Yang, M. Li, F. Ren, T. Imran, Z. Sun, S. Zhang, Y. Zhang, Z. Zhao, Z. Liu, W. Chen, *J. Energy Chem.* **2023**, *80*, 689.
- [29] P. Wang, Y. Wu, B. Cai, Q. Ma, X. Zheng, W. H. Zhang, *Adv. Funct. Mater.* **2019**, *29*, 1807661.
- [30] D. Castro, V. C. M. Duarte, L. Andrade, *ACS Omega* **2022**, *7*, 40844.
- [31] J. Werner, C. C. Boyd, T. Moot, E. J. Wolf, R. M. France, S. A. Johnson, M. F. A. M. Hest, J. M. Luther, K. Zhu, J. J. Berryb, M. D. McGehee, *Energy Environ. Sci.* **2020**, *13*, 3393.
- [32] L. Gao, L. Chen, S. Huang, X. Li, G. Yang, *ACS Appl. Energy Mater.* **2019**, *2*, 3851.
- [33] J. H. Kim, S. T. Williams, N. Cho, C. C. Chueh, A. K. Y. Jen, *Adv. Energy Mater.* **2015**, *5*, 2.
- [34] W. Q. Wu, Z. Yang, P. N. Rudd, Y. Shao, X. Dai, H. Wei, J. Zhao, Y. Fang, Q. Wang, Y. Liu, Y. Deng, X. Xiao, Y. Feng, J. Huang, *Sci. Adv.* **2019**, *5*, 1.
- [35] C. Li, J. Yin, R. Chen, X. Lv, X. Feng, Y. Wu, J. Cao, *J. Am. Chem. Soc.* **2019**, *141*, 6345.
- [36] K. M. Lee, C. H. Lai, W. C. Chu, S. H. Chan, V. Suryanarayanan, *Sol. Energy* **2020**, *204*, 337.
- [37] S. H. Huang, K. Y. Tian, H. C. Huang, C. F. Li, W. C. Chu, K. M. Lee, Y. C. Huang, W. F. Su, *ACS Appl. Mater. Interfaces* **2020**, *12*, 26041.
- [38] S. Qiu, X. Xu, L. Zeng, Z. Wang, Y. Chen, C. Zhang, C. Li, J. Hu, T. Shi, Y. Mai, F. Guo, *J. Energy Chem.* **2020**, *54*, 45.
- [39] Z. Huang, X. Hu, Z. Xing, X. Meng, X. Duan, J. Long, T. Hu, L. Tan, Y. Chen, *J. Phys. Chem. C* **2020**, *124*, 8129.
- [40] J. Zhang, T. Bu, J. Li, H. Li, Y. Mo, Z. Wu, Y. Liu, X. L. Zhang, Y. B. Cheng, F. Huang, *J. Mater. Chem. A* **2020**, *8*, 8447.
- [41] S. Razza, F. D. Giacomo, F. Matteocci, L. Cinà, A. L. Palma, S. Casaluci, P. Cameron, A. D'Epifanio, S. Licoccia, A. Reale, T. M. Brown, A. Di Carlo, *J. Power Sources* **2015**, *277*, 286.
- [42] J. Li, R. Munir, Y. Fan, T. Niu, Y. Liu, Y. Zhong, Z. Yang, Y. Tian, B. Liu, J. Sun, D. M. Smilgies, S. Thoroddsen, A. Amassian, K. Zhao, S. (F.) Liu, *Joule* **2018**, *2*, 1313.
- [43] X. Xu, Z. Liu, Z. Zuo, M. Zhang, Z. Zhao, Y. Shen, H. Zhou, Q. Chen, Y. Yang, M. Wang, *Nano Lett.* **2015**, *15*, 2402.
- [44] Y. Deng, Q. Dong, C. Bi, Y. Yuan, J. Huang, *Adv. Energy Mater.* **2016**, *6*, 1.
- [45] Q. Wei, Z. Ye, X. Ren, F. Fu, Z. Yang, S. (F) Liu, D. Yang, *Sci. China Chem.* **2020**, *63*, 818.
- [46] Y. Zhong, R. Munir, J. Li, M. C. Tang, M. R. Niazi, D. M. Smilgies, K. Zhao, A. Amassian, *ACS Energy Lett.* **2018**, *3*, 1078.
- [47] M. Ernst, J. P. Herterich, C. Margenfeld, M. Kohlstädte, U. Würfel, *Sol. RRL* **2022**, *6*, 2100535.
- [48] F. Matteocci, L. Vesce, F. U. Kosasih, L. A. Castriotta, S. Cacovich, A. L. Palma, G. Divitini, C. Ducati, A. D. Carlo, *ACS Appl. Mater. Interfaces* **2019**, *11*, 25195.
- [49] F. Mohamadkhani, S. Javadpour, N. Taghavinia, *Sol. Energy* **2019**, *191*, 647.
- [50] F. Mohamadkhani, M. Heidariramsheh, S. Javadpour, E. Ghavaminia, S. M. Mahdavi, N. Taghavinia, *Sol. Energy* **2021**, *223*, 106.
- [51] S. Wang, Z. Ma, B. Liu, W. Wu, Y. Zhu, R. Ma, C. Wang, *Sol. RRL* **2018**, *2*, 180034.

- [52] Z. Wang, L. Zeng, C. Zhang, Y. Lu, S. Qiu, C. Wang, C. Liu, L. Pan, S. Wu, J. Hu, G. Liang, P. Fan, H. J. Egelhaaf, C. J. Brabec, F. Guo, Y. Mai, *Adv. Funct. Mater.* **2020**, *30*, 2001240.
- [53] E. Aydin, M. D. Bastiani, S. D. Wolf, *Adv. Mater.* **2019**, *31*, 1.
- [54] B. Chen, P. N. Rudd, S. Yang, Y. Yuanc, J. Huang, *Chem. Soc. Rev.* **2019**, *48*, 3842.
- [55] S. Yang, J. Dai, Z. Yu, Y. Shao, Y. Zhou, X. Xiao, X. C. Zeng, J. J. J. Huang, *J. Am. Chem. Soc.* **2019**, *141*, 5781.
- [56] S. C. Hermosa, L. Wouk, I. S. Bicalho, L. Q. de Corrêa, B. J. L. Cinà, T. M. Brownm, D. Bagnis, *Nano Res.* **2021**, *14*, 1034.
- [57] M. Yang, D. H. Kim, T. R. Klein, Z. Li, M. O. Reese, B. J. T. Villers, J. J. Berry, M. F. A. M. Hest, K. Zhu, *ACS Energy Lett.* **2018**, *3*, 322.
- [58] Y. Deng, C. H. V. Brackle, X. Dai, J. Zhao, B. Chen, J. Huang, *Sci. Adv.* **2019**, *5*, eaax7537.
- [59] X. Dai, Y. Deng, C. H. V. Brackle, S. Chen, P. N. Rudd, X. Xiao, Y. Lin, B. Chen, J. Huang, *Adv. Energy Mater.* **2020**, *10*, 1903108.
- [60] J. W. Yoo, J. Jang, U. Kim, S. G. Ji, E. Noh, S. Hong, M. Choi, S. I. Seok, *Joule* **2021**, *5*, 2420.
- [61] M. Yang, D. H. Kim, T. R. Klein, Z. Li, M. O. Reese, B. J. Tremolet De Villers, J. J. Berry, M. F. A. M. Van Hest, K. Zhu, *ACS Energy Lett.* **2018**, *3*, 322.
- [62] L. Vesce, M. Stefanelli, F. Rossi, L. A. Castriotta, B. Riccardo, M. L. Parisi, A. Sinicropi, A. Di Carlo, *Prog. Photovolt. Res. Appl.* **2024**, *32*, 115.
- [63] S. Castro-Hermosa, L. Wouk, I. S. Bicalhoa, L. Q. de Corrêa, B. de Jong, L. Cinà, T. M. Brown, D. Bagnisa, *Nano Res.* **2021**, *14*, 1034.
- [64] Z. Bi, X. Xu, X. Chen, Y. Zhu, C. Liu, H. Yu, Y. Zheng, P. A. Troshin, A. Guerrero, G. Xu, *Chem. Eng. J.* **2022**, *446*, 137164.
- [65] J. Zeng, L. Bi, Y. Cheng, B. Xu, A. K. Y. Jen, *Nano Res. Energy* **2022**, *1*, 9120004.
- [66] M. Abbas, M. Rauf, B. Cai, F. Guo, X. C. Yuan, T. R. Rana, J. D. Mackenzie, A. K. K. Kyaw, *ACS Appl. Energy Mater.* **2023**, *6*, 6485.
- [67] Y. Ding, B. Ding, H. Kanda, O. J. Usiobo, T. Gallet, Z. Yang, Y. Liu, H. Huang, J. Sheng, C. Liu, Y. Yang, V. I. E. Queloz, X. Zhang, J. N. Audinot, A. Redinger, W. Dang, E. Mosconic, W. Luo, F. D. Angelis, M. Wang, P. Dörflinger, M. Armer, V. Schmid, R. Wang, M. K. Nazeeruddin, *Nat. Nanotechnol.* **2022**, *17*, 598.
- [68] M. C. Tang, Y. Fan, D. Barrit, X. Chang, H. X. Dang, R. Li, K. Wang, D. M. Smilgies, S. (F) Liu, S. D. Wolf, T. D. Anthopoulos, K. Zhao, A. Amassian, *J. Mater. Chem. A* **2020**, *8*, 1095.
- [69] M. Konstantakou, D. Perganti, P. Falaras, T. Stergiopoulos, *Crystals* **2017**, *7*, 291.
- [70] X. Li, D. Bi, C. Yi, J. D. Décoppet, J. Luo, S. M. Zakeeruddin, A. Hagfeldt, M. Grätzel, *Science* **2016**, *353*, 58.
- [71] F. Huang, Y. Dkhissi, W. Huang, M. Xiao, I. Benesperi, S. Rubanov, Y. Zhu, X. Lin, L. Jiang, Y. Zhou, A. Gray-Weale, J. Etheridge, C. R. McNeill, R. A. Caruso, U. Bach, L. Spiccia, Y. B. Cheng, *Nano Energy* **2014**, *10*, 10.
- [72] Y. Y. Kim, T. Y. Yang, R. Suhonen, M. Välimäki, T. Maaninen, A. Kemppainen, N. J. Jeon, J. Seo, *Adv. Sci.* **2019**, *6*, 1802094.
- [73] A. C. B. Luszczynska, B. G. R. Dupont, Z. Sieradzki, *Display Imaging* **2017**, *2*, 339.
- [74] P. Maisch, K. C. Tam, D. J. Jang, M. Steinberger, F. Yang, C. J. Brabec, H. J. Egelhaaf, *Organic Flexible Electronics*, Woodhead Publishing, Cambridge **2021**, pp. 305–333.
- [75] F. Mathies, E. J. W. List-Kratochvil, E. L. Unger, *Energy Technol.* **2020**, *8*, 1900991.
- [76] X. Peng, J. Yuan, S. Shen, M. Gao, A. S. R. Chesman, H. Yin, J. Cheng, Q. Zhang, D. Angmo, *Adv. Funct. Mater.* **2017**, *27*, 1703704.
- [77] H. Eggers, F. Schackmar, T. Abzieher, Q. Sun, U. Lemmer, Y. Vaynzof, B. S. Richards, G. Hernandez-Sosa, U. W. Paetzold, *Adv. Energy Mater.* **2019**, *10*, 1903184.
- [78] S. K. Karunakaran, G. M. Arumugam, W. Yang, S. Ge, S. N. Khan, X. Lin, G. Yang, *J. Mater. Chem. A* **2019**, *7*, 13873.
- [79] Z. Wei, H. Chen, K. Yan, S. Yang, *Angew. Chem., Int. Ed.* **2014**, *53*, 13239.
- [80] S. G. Li, K. J. Jiang, M. J. Su, X. P. Cui, J. H. Huang, Q. Q. Zhang, X. Q. Zhou, L. M. Yang, Y. L. Song, *J. Mater. Chem. A* **2015**, *3*, 9092.
- [81] M. Bag, Z. Jiang, L. A. Renna, S. P. Jeong, V. M. Rotello, D. Venkataraman, *Mater. Lett.* **2016**, *164*, 472.
- [82] S. G. Hashmi, A. Tiihonen, D. Martineau, M. Ozkan, P. Vivo, K. Kaunisto, V. Ulla, S. M. Zakeeruddin, M. Grätzel, *J. Mater. Chem. A* **2017**, *5*, 4797.
- [83] Z. Jiang, M. Bag, L. A. Renna, S. P. Jeong, V. M. Rotello, D. Venkataraman, *HAL* **2016**, *1*, 01386295.
- [84] F. Mathies, T. Abzieher, A. Hochstuhl, K. Glaser, A. Colsmann, U. W. Paetzold, G. Hernandez-Sosa, U. Lemmer, A. Quintilla, *J. Mater. Chem. A* **2016**, *4*, 19207.
- [85] F. Mathies, H. Eggers, B. S. Richards, G. Hernandez-Sosa, U. Lemmer, U. W. Paetzold, *ACS Appl. Energy Mater.* **2018**, *1*, 1834.
- [86] N. Ahn, D. Y. Son, I. H. Jang, S. M. Kang, M. Choi, N. G. Park, *Am. Chem. Soc.* **2015**, *137*, 8696.
- [87] C. Liang, P. Li, H. Gu, Y. Zhang, F. Li, Y. Song, G. Shao, N. Mathews, G. Xing, *Sol. RRL* **2018**, *2*, 1700217.
- [88] P. Li, C. Liang, B. Bao, Y. Li, X. Hu, Y. Wang, Y. Zhang, F. Li, G. Shao, Y. Song, *Nano Energy* **2018**, *46*, 203.
- [89] S. Schlisske, F. Mathies, D. Busko, N. Strobel, T. Rödlmeier, B. S. Richards, U. Lemmer, U. W. Paetzold, G. Hernandez-Sosa, E. Klampaftis, *ACS Appl. Energy Mater.* **2019**, *2*, 764.
- [90] Z. Li, P. Li, G. Chen, Y. Cheng, X. Pi, X. Yu, D. Yang, L. Han, Y. Zhang, Y. Song, *ACS Appl. Mater. Interfaces* **2020**, *12*, 39082.
- [91] F. Schackmar, H. Eggers, M. Frericks, B. S. Richards, U. Lemmer, G. Hernandez-Sosa, U. W. Paetzold, *Adv. Mater. Technol.* **2021**, *6*, 2000271.
- [92] C. S. Pathak, G. Paramasivam, F. Mathies, K. Hirselandt, V. Schröder, O. Maus, J. Dagar, C. Klimm, E. Unger, I. Visoly-Fisher, *ACS Appl. Energy Mater.* **2022**, *5*, 4085.
- [93] H. Yang, J. Wang, X. Yu, Y. Feng, X. Chen, F. Long, Z. Ku, F. Huang, Y. Cheng, Y. Peng, *Chem. Phys. Lett.* **2022**, *807*, 14008.
- [94] T. Okoroafor, A. Maalouf, S. Oez, V. Babu, B. Wilk, S. Resalati, *J. Clean. Prod.* **2022**, *373*, 133665.
- [95] K. Xu, A. Al-Ashouri, Z. W. Peng, E. Köhnen, H. Hempel, F. Akhundova, J. A. Marquez, P. Tockhorn, O. Shargaeva, F. Ruske, J. Zhang, J. Dagar, B. Stannowski, T. Unold, D. Abou-Ras, E. Unger, L. Korte, S. Albrecht, *ACS Energy Lett.* **2022**, *7*, 3600.
- [96] B. Parida, Ar. Singh, A. K. K. Soopy, S. Sangaraju, M. Sundaray, S. Mishra, S. (F) Liu, A. Najar, *Adv. Sci.* **2022**, *9*, 2200308.
- [97] Z. Wan, M. Xu, Z. Fu, D. Li, A. Mei, Y. Hu, Y. Rong, H. Han, *Front. Optoelectron.* **2019**, *12*, 344.
- [98] S. Alon, M. Sohmer, Ch. S. Pathak, I. V. Fisher, L. Etgar, *Sol. RRL* **2021**, *5*, 2100028.
- [99] Z. Ku, Y. Rong, M. Xu, T. Liu, H. Han, *Sci. Rep.* **2013**, *3*, 3132.
- [100] Y. Rong, Z. Ku, A. Mei, T. Liu, M. Xu, S. Ko, X. Li, H. Han, *J. Phys. Chem. Lett.* **2014**, *5*, 2160.
- [101] C. Y. Chan, Y. Wang, G. W. Wu, E. W. G. Diau, *J. Mater. Chem. A* **2016**, *4*, 3872.
- [102] Y. Sheng, W. Ji, Y. Chu, Y. Ming, A. Mei, Y. Hu, Y. Rong, H. Han, *Sol. RRL* **2020**, *4*, 2000185.
- [103] D. Raptis, C. A. Worsley, S. M. P. Meroni, A. Pockett, M. Carnie, T. Watson, *Solar* **2022**, *2*, 293.
- [104] C. Chen, J. Chen, H. Han, L. Chao, J. Hu, T. Niu, H. Dong, S. Yang, Y. Xia, Y. Chen, W. Huang, *Nature* **2022**, *612*, 266.

- [105] B. A. Kamino, B. Paviet-Salomon, S. J. Moon, N. Badel, J. Levrat, G. Christmann, A. Walter, A. Faes, L. Ding, J. J. D. Leon, A. Paracchino, M. Despeisse, C. Ballif, S. Nicolay, *ACS Appl. Energy Mater.* **2019**, 2, 3815.
- [106] Y. Tu, J. Ye, G. Yang, Y. Zang, L. Zhang, Y. Wang, G. Li, L. Chu, W. Yan, *J. Alloys Compd.* **2023**, 942, 169104.
- [107] Y. Rong, Y. Ming, W. Ji, D. Li, A. Mei, Y. Hu, H. Han, *J. Phys. Chem. Lett.* **2018**, 9, 2707.
- [108] O. J. Romero, L. E. Scriven, M. S. Carvalho, J. Nonnewton, *Fluid Mech.* **2006**, 138, 63.
- [109] S. Razza, S. Castro-Hermosa, A. Di Carlo, T. M. Brown, *APL Mater.* **2016**, 4, 091508.
- [110] D. Burkitt, J. Searle, D. A. Worsley, T. Watson, *Materials* **2018**, 11, 2106.
- [111] I. Zimmermann, M. A. Atem, O. Fournier, S. Bernard, S. Jutteau, L. Lombez, J. Rousset, *Adv. Mater. Interfaces* **2021**, 8, 1.
- [112] C. Gong, S. Tong, K. Huang, H. Li, H. Huang, J. Zhang, J. Yang, *Sol. RRL* **2020**, 4, 1.
- [113] H. Li, C. Zuo, D. Angmo, H. Weerasinghe, M. Gao, J. Yang, *Nano-Micro Lett.* **2022**, 14, 79.
- [114] G. Cotella, J. Baker, D. Worsley, F. DeRossi, C. P. Pearce, M. Carnie, T. Watson, *Sol. Energy Mater. Sol. Cells* **2017**, 159, 362.
- [115] J. E. Kim, Y. S. Jung, Y. J. Heo, K. Hwang, T. Qin, D. Y. Kim, D. Vak, *Sol. Energy Mater. Sol. Cells* **2018**, 179, 80.
- [116] F. Bisconti, A. Giuri, G. Marra, A. Savoini, P. Fumo, R. Marrazzo, S. Zanardi, G. Corso, R. Po, P. Biagini, E. Quadrivi, R. Suuronen, T. M. Kraft, M. Ylikurnari, A. Listorti, C. E. Corcione, S. Colella, A. Rizzo, *ChemPlusChem* **2021**, 86, 1442.
- [117] T. M. Schmidt, T. T. Larsen-Olsen, J. E. Carlé, D. Angmo, F. C. Krebs, *Adv. Energy Mater.* **2015**, 5, 1.
- [118] Z. Gu, L. Zuo, T. T. Larsen-Olsen, T. Ye, G. Wu, F. C. Krebs, H. Chen, *J. Mater. Chem. A* **2015**, 3, 24254.
- [119] T. Qin, W. Huang, J. E. Kim, D. Vak, C. Forsyth, C. R. McNeill, Y. B. Cheng, *Nano Energy* **2017**, 31, 210.
- [120] J. Ciro, M. A. Mejía-Escobar, F. Jaramillo, *Sol. Energy* **2017**, 150, 570.
- [121] B. J. Huang, C. K. Guan, S. H. Huang, W. F. Su, *Sol. Energy* **2020**, 205, 192.
- [122] M. Fievez, P. J. S. Rana, T. M. Koh, M. Manceau, J. H. Lew, N. F. Jamaludin, B. Ghosh, A. Bruno, S. Cros, S. Berson, S. G. Mhaisalkar, W. L. Leong, *Sol. Energy Mater. Sol. Cells* **2021**, 230, 111189.
- [123] K. Hwang, Y. S. Jung, Y. J. Heo, F. H. Scholes, S. E. Watkins, J. Subbiah, D. J. Jones, D. Y. Kim, D. Vak, *Adv. Mater.* **2015**, 27, 1241.
- [124] K. Hwang, Y. S. Jung, Y. J. Heo, F. Scholes, S. E. Watkins, J. Subbiah, D. J. Jones, D. Kim, D. Vak, *Adv. Mater.* **2015**, 7, 1241.
- [125] M. Xu, W. Ji, Y. Sheng, Y. Wu, H. Cheng, J. Meng, Z. Yan, J. Xu, A. Mei, Y. Hu, Y. Rong, H. Han, *Nano Energy* **2020**, 74, 1.
- [126] D. Seok Ham, W. Jin Choi, H. Yun, M. Kim, D. H. Yeo, S. Lee, B. J. Kim, J. H. Lee, *ACS Appl. Energy Mater.* **2021**, 4, 7611.
- [127] Y. Galagan, F. D. Giacomo, H. Gorter, G. Kirchner, I. D. Vries, R. Andriessen, P. Groen, *Adv. Energy Mater.* **2018**, 8, 1.
- [128] D. Burkitt, R. Patidar, P. Greenwood, K. Hooper, J. McGettrick, S. Dimitrov, M. Colombo, V. Stoichkov, D. Richards, D. Beynon, M. Davies, T. Watson, *Sustain. Energy Fuels* **2020**, 4, 3340.
- [129] Z. Yang, W. Zhang, S. Wu, H. Zhu, Z. Liu, Z. Liu, Z. Jiang, R. Chen, J. Zhou, Q. Lu, Z. Xia, L. Shi, H. Chen, L. K. Ono, S. Zhang, Y. Zhang, Y. Qi, L. Han, W. Chen, *Sci. Adv.* **2021**, 7, 1.
- [130] W. Nie, H. Tsai, R. Asadpour, J. C. Blancon, A. J. Neukirch, G. Gupta, J. J. Crochet, M. Chhowalla, S. Tretiak, M. A. Alam, H. L. Wang, A. D. Mohite, *Science* **2015**, 347, 522.
- [131] Y. Rong, Z. Tang, Y. Zhao, X. Zhong, S. Venkatesan, H. Graham, M. Patton, Y. Jing, A. M. Guloy, Y. Yao, *Nanoscale* **2015**, 7, 10595.
- [132] F. Huang, Y. Dkhissi, W. Huang, M. Xiao, I. Benesperi, S. Rubanov, Y. Zhu, X. Lin, L. Jiang, Y. Zhou, A. G. Weale, J. Etheridge, C. R. McNeill, R. A. Caruso, U. Bach, L. Spiccia, Y. B. Cheng, *Nano Energy* **2014**, 10, 10.
- [133] Y. J. Jeon, S. Lee, R. Kang, J. E. Kim, J. S. Yeo, S. H. Lee, S. S. Kim, J. M. Yun, D. Y. Kim, *Sci. Rep.* **2014**, 4, 6953.
- [134] J. H. Heo, D. H. Song, H. J. Han, S. Y. Kim, J. H. Kim, D. Kim, H. W. Shin, T. K. Ahn, C. Wolf, T. W. Lee, S. H. Im, *Adv. Mater.* **2015**, 27, 3424.
- [135] C. Y. Chang, C. Y. Chu, Y. C. Huang, C. W. Huang, S. Y. Chang, C. A. Chen, C. Y. Chao, W. F. Su, *ACS Appl. Mater. Interfaces* **2015**, 7, 4955.
- [136] X. Li, M. I. Dar, C. Yi, J. Luo, M. Tschumi, S. M. Zakeeruddin, M. K. Nazeeruddin, H. Han, M. Grätzel, *Nat. Chem.* **2015**, 7, 703.
- [137] S. Bernard, S. Jutteau, S. Mejaouri, S. Cacovich, I. Zimmermann, A. Yaiche, S. Gbegnon, D. Loisnard, S. Collin, A. Duchatelet, F. Sauvage, J. Rousset, *Sol. RRL* **2021**, 5, 2100391.
- [138] Y. S. Jung, K. Hwang, Y. J. Heo, J. E. Kim, D. Lee, C. H. Lee, H. I. Joh, J. S. Yeo, D. Y. Kim, *ACS Appl. Mater. Interfaces* **2017**, 9, 27832.
- [139] Y. Y. Kim, E. Y. Park, T. Y. Yang, J. H. Noh, T. J. Shin, N. J. Jeon, J. Seo, *J. Mater. Chem. A* **2018**, 6, 12447.
- [140] Q. Wang, *Phys. Chem. Chem. Phys.* **2018**, 20, 10114.
- [141] E. Raza, F. Aziz, Z. Ahmad, *RSC Adv.* **2018**, 8, 20952.
- [142] A. Verma, D. Martineau, E. Hack, M. Makha, E. Turner, F. Nüesch, J. Heier, *J. Mater. Chem. C* **2020**, 8, 6124.
- [143] F. Xu, J. Liu, A. S. Subbiah, W. Liu, J. Kang, G. T. Harrison, X. Yang, F. H. Isikgor, E. Aydin, M. D. Bastiani, S. D. Wolf, *Small Sci.* **2021**, 1, 2000044.
- [144] S. Y. Abate, Z. Yang, S. Jha, G. Ma, Z. Ouyang, H. Zhang, S. Muhammad, N. Pradhan, X. Gu, D. Patton, K. Wang, D. Li, J. Cai, Q. Dai, *Chem. Eng. J.* **2023**, 457, 141199.
- [145] F. Di Giacomo, S. Shanmugam, H. Fledderus, B. J. Bruijnaers, W. J. H. Verhees, M. S. Dorenkamper, S. C. Veenstra, W. Qiu, R. Gehlhaar, T. Merckx, T. Aernouts, R. Andriessen, Y. Galagan, *Sol. Energy Mater. Sol. Cells* **2018**, 181, 53.
- [146] M. Du, X. Zhu, L. Wang, H. Wang, J. Feng, X. Jiang, Y. Cao, Y. Sun, L. Duan, Y. Jiao, K. Wang, X. Ren, Z. Yan, S. Pang, S. (Frank) Liu, *Adv. Mater.* **2020**, 32, 2004979.
- [147] J. Li, J. Dagar, O. Shargaiya, M. A. Flatken, H. Köbler, M. Fenske, C. Schultz, B. Stegemann, J. Just, D. M. Többens, A. Abate, R. Munir, E. Unger, *Adv. Energy Mater.* **2021**, 11, 2003460.
- [148] J. Li, J. Dagar, O. Shargaiya, O. Maus, M. Remec, Q. Emery, M. Khenkin, C. Ulbrich, F. Akhundova, J. A. Márquez, T. Unold, M. Fenske, C. Schultz, B. Stegemann, A. Al-Ashouri, S. Albrecht, A. T. Esteves, L. Korte, H. Köbler, A. Abate, D. M. Többens, I. Zizak, E. J. W. List-Kratochvil, R. Schlatmann, E. Unger, *Adv. Energy Mater.* **2023**, 13, 203898.
- [149] T. S. Le, D. Saranin, P. Gostishchev, I. Ermanova, T. Komaricheva, L. Luchnikov, D. Muratov, A. Uvarov, E. Vyacheslavova, I. Mukhin, S. Didenko, D. Kuznetsov, A. Di Carlo, *Sol. RRL* **2022**, 6, 2100807.
- [150] V. Nguyen, P. Dally, I. Zimmermann, **2022**, <https://doi.org/10.4229/WCPEC-82022-2AV.1.20>.
- [151] C. F. Li, H. C. Huang, S. H. Huang, Y. H. Hsiao, P. Chaudhary, C. Y. Chang, F. Y. Tsai, W. F. Su, Y. C. Huang, *Nanomaterials* **2023**, 13, 1760.
- [152] J. E. Bishop, J. A. Smith, D. G. Lidzey, *ACS Appl. Mater. Interfaces* **2020**, 12, 48237.
- [153] J. E. Bishop, D. K. Mohamad, M. Wong-Stringer, A. Smith, D. G. Lidzey, *Sci. Rep.* **2017**, 7, 7962.
- [154] C. Girotto, D. Moia, B. P. Rand, P. Heremans, *Adv. Funct. Mater.* **2011**, 21, 64.
- [155] M. Eslamian, *Coatings* **2014**, 4, 60.

- [156] K. M. Boopathi, M. Ramesh, P. Perumal, Y. C. Huang, C. S. Tsao, Y. F. Chen, C. H. Lee, C. W. Chu, *J. Mater. Chem.* **2015**, *3*, 9257.
- [157] F. Li, C. Bao, H. Gao, W. Zhu, T. Yu, J. Yang, G. Fu, X. Zhou, Z. Zou, *Mater. Lett.* **2015**, *157*, 38.
- [158] X. Xia, W. Wu, H. Li, B. Zheng, Y. Xue, J. Xu, D. Zhang, C. Gao, X. Liu, *RSC Adv.* **2016**, *6*, 14792.
- [159] C. F. J. Lau, X. Deng, Q. Ma, J. Zheng, J. S. Yun, M. A. Green, S. Huang, A. W. Y. Ho-Baillie, *ACS Energy Lett.* **2016**, *1*, 573.
- [160] G. Chai, S. Luo, H. Zhou, W. A. Daoud, *Mater. Des.* **2017**, *125*, 222.
- [161] H. Huang, J. Shi, L. Zhu, D. Li, Y. Luo, Q. Meng, *Nano Energy* **2016**, *27*, 352.
- [162] Y. Jiang, M. Remeika, Z. Hu, E. J. Juarez-Perez, L. Qiu, Z. Liu, T. Kim, L. K. Ono, D.-Y. Son, Z. Hawash, M. R. Leyden, Z. Wu, L. Meng, J. Hu, Y. Qi, *Adv. Energy Mater.* **2019**, *9*, 1803047.
- [163] A. T. Barrows, A. J. Pearson, C. K. Kwak, A. D. F. Dunbar, A. R. Buckley, D. G. Lidzey, *Energy Environ. Sci.* **2014**, *7*, 2944.
- [164] S. Das, B. Yang, G. Gu, P. C. Joshi, I. N. Ivanov, C. M. Rouleau, T. Aytug, D. B. Geohegan, K. Xiao, *ACS Photonics* **2015**, *2*, 680.
- [165] J. G. Tait, S. Manghooli, W. Qiu, L. Rakocevic, L. Kootstra, M. Jaysankar, C. A. Masse de la Huerta, U. W. Paetzold, R. Gehlhaar, D. Cheyns, P. Heremans, J. Poortmans, *J. Mater. Chem. A* **2016**, *4*, 3792.
- [166] J. H. Heo, M. H. Lee, M. H. Jang, S. H. Im, *J. Mater. Chem. A* **2016**, *4*, 17636.
- [167] J. E. Bishop, J. A. Smith, Cl. Greenland, V. Kumar, N. Vaenas, O. S. Game, T. J. Routledge, M. Wong-Stringer, C. Rodenburg, D. G. Lidzey, *ACS Appl. Mater. Interfaces* **2018**, *10*, 39428.
- [168] J. Su, H. Cai, J. Yang, X. Ye, R. Han, J. Ni, J. Li, J. Zhang, *ACS Appl. Mater. Inter* **2020**, *12*, 3531.
- [169] H. Cai, X. Liang, X. Ye, J. Su, J. Guan, J. Yang, Y. Liu, X. Zhou, R. Han, J. Ni, J. Li, J. Zhang, *ACS Appl. Energy Mater.* **2020**, *3*, 9696.
- [170] J. E. Bishop, C. D. Read, J. A. Smith, T. J. Routledge, D. G. Lidzey, *Sci. Rep.* **2020**, *10*, 6610.
- [171] J. E. Bishop, T. J. Routledge, D. G. Lidzey, *J. Phys. Chem. Lett.* **2018**, *9*, 1977.
- [172] M. Liu, M. B. Johnston, H. J. Snaith, *Nature* **2013**, *501*, 395.
- [173] G. Tong, X. Geng, Y. Yu, L. Yu, J. Xu, Y. Jiang, Y. Sheng, Y. Shi, K. Chen, *RSC Adv.* **2017**, *7*, 18224.
- [174] J. Li, H. Wang, X. Y. Chin, H. A. Dewi, K. Vergeer, T. W. Goh, J. W. M. Lim, J. H. Lew, K. P. Loh, C. Soci, T. C. Sum, H. J. Bolink, N. Mathews, S. Mhaisalkar, A. Bruno, *Joule* **2020**, *4*, 1035.
- [175] D. Lin, Y. Gao, T. Zhang, N. Pang, Z. Wu, K. Chen, T. Shi, Z. Pan, P. Liu, W. Xie, *Adv. Funct. Mater.* **2022**, *32*, 2208392.
- [176] S. Wang, L. Tan, J. Zhou, M. Li, X. Zhao, H. Li, W. Tress, L. Ding, M. Graetzel, C. Yi, *Joule* **2022**, *6*, 1344.
- [177] H. Li, J. Zhou, L. Tan, M. Li, C. Jiang, S. Wang, X. Zhao, Y. Liu, Y. Zhang, Y. Ye, W. Tress, C. Yi, *Sci. Adv.* **2022**, *8*, eab07422.



Azam Khorasani is a postdoctoral researcher at Abdullah Gul University, Turkey. She earned her Ph.D. in solid-state physics from Arak University, Arak, Iran. Her research primarily revolves around nanotechnology, with a specific focus on perovskite nanocrystals and materials, solar cells, and light-emitting diodes. Dr. Khorasani aims to pioneer the development of cost-effective and highly efficient perovskite nanocrystals, improve their stability, and apply them in the fabrication of large-area devices.



Fateme Mohammakhani received her Ph.D. in materials science and engineering from Shiraz University, Shiraz, Iran, in 2020. Her doctoral thesis focused on the fabrication and optimization of perovskite solar cells through the implementation of novel electron transport layers and hole transport layers. Her current research interests include nanomaterials and thin films for applications in energy and environmental technologies.



Maziar Marandi is an associate professor of physics at Arak University. He earned his Ph.D. in applied physics and nanophysics in 2007 from Sharif University of Technology. Following his graduation, he served as a postdoctoral researcher at Sharif University for 2 years. Currently, he holds the position of the head of Arak University's physics department. Dr. Marandi's research focuses on nanostructures, quantum dot-sensitized solar cells, experimental and theoretical perovskite solar cells, and dye-sensitized solar cells. With over 30 master's students and four Ph.D. students under his supervision, he has authored more than 60 ISI papers published in well-known journals.



Huiming Luo is currently a Ph.D. student in the Functional Materials and Energy Device Research Group (FMED) at the Institute for Materials Discovery in University College London. She earned her M.Sc. from South China University of Technology in 2022 and her B.Sc. in environmental engineering from Nanjing Forestry University in 2019. Her current research focuses on the development of ecofriendly optoelectronic devices, particularly solar cells, and light-emitting diodes, based on metal halide perovskites and double perovskites.



Mojtaba Abdi-Jalebi is an associate professor in energy and functional materials in the Institute for Materials Discovery, University College London. He completed his Ph.D. in physics at Cavendish Laboratory, University of Cambridge. From 2018 to 2020, he was a junior research fellow at Wolfson College in Cambridge. His research focuses on the development of emerging semiconductors for low-cost optoelectronic and electrochemical devices for low-cost electronics applications and energy systems enabling carbon capture and production of solar fuels. His research aims to develop and incorporate new inexpensive materials in energy devices to alter the energy landscape by reducing the cost of energy production, consumption, and storage.